Colorectal cancer triple co-culture spheroid model to assess the biocompatibility and anticancer properties of polymeric nanoparticles

Tomás Bauleth Ramos, Tália Feijão, André Gonçalves, Mohammad Ali Shahbazi, Zehua Liu, Cristina Barrias, Maria José Oliveira, Pedro Granja, Hélder A. Santos, Bruno Sarmento

PII: S0168-3659(20)30238-8

DOI: https://doi.org/10.1016/j.jconrel.2020.04.025

Reference: COREL 10278

To appear in: *Journal of Controlled Release*

Received date: 29 December 2019

Revised date: 14 April 2020

Accepted date: 15 April 2020

Please cite this article as: T.B. Ramos, T. Feijão, A. Gonçalves, et al., Colorectal cancer triple co-culture spheroid model to assess the biocompatibility and anticancer properties of polymeric nanoparticles, *Journal of Controlled Release* (2020), https://doi.org/10.1016/j.jconrel.2020.04.025

Colorectal Cancer Triple Co-culture Spheroid Model to Assess the Biocompatibility and Anticancer Properties of Polymeric Nanoparticles

Tomás Bauleth-Ramos[a,b,c,d]*, Tália Feijão[a,b], André Gonçalves[a,b,c,e], Mohammad-Ali Shahbazi[d,f], Zehua Liu[d], Cristina Barrias[a,b,c], Maria José Oliveira[a,b,g], Pedro Granja[a,b,c], Hélder A. Santos[d,h]*, Bruno Sarmento[a,b,i]*

[a]Instituto de Investigação e Inovação em Saúde (i3S), University of Porto, Rua Alfredo Allen, 208, 4200-135, Porto, Portugal
[b]Instituto de Engenharia Biomédica (INEB), University of Porto, Rua Alfredo Allen, 208, 4200-135, Porto, Portugal
[c]Instituto Ciências Biomédicas Abel Salazar (ICBAS), University of Porto, Rua Jorge Viterbo 228, 4150-180, Porto, Portugal
[d]Drug Research Program, Division of Pharmaceutical Chemistry and Technology, Faculty of Pharmacy, University of Helsinki, FI-00014, Helsinki, Finland
[e]Faculdade de Engenharia da Universidade do Porto (FEUP), University of Porto, Rua Dr. Roberto Frias, 4200-465, Porto, Portugal
[f]Department of Pharmaceutical Nanotechnology, School of Pharmacy, Zanjan University of Medical Sciences, 56184-45139 Zanjan, Iran
[g]Departmento de Patologia e Oncologia, Faculdade de Medicina, University of Porto, Alameda Prof. Hernâni Monteiro, 4200-319, Porto, Portugal
[h]Helsinki Institute of Life Science, University of Helsinki, FI-00014, Helsinki, Finland
[i]CESPU, Instituto de Investigação e Formação Avançada em Ciências e Tecnologias da Saúde, Rua Central da Gandra 1317, 4585-116, Gandra, Portugal

Email: bruno.sarmento@ineb.up.pt; tomas.ramos@i3s.up.pt; helder.santos@helsinki.fi

Abstract

Colorectal cancer (CRC) is the third most common and the second deadliest type of cancer worldwide, urging the development of more comprehensive models and of more efficient treatments. Although the combination of nanotechnology with chemo- and immuno-therapy has represented a promising treatment approach, its translation to the clinic has been hampered by the absence of cellular models that can provide reliable and predictive knowledge about the *in vivo* efficiency of the formulation. Herein, a 3D model based on CRC multicellular tumor spheroids (MCTS) model was developed by combining epithelial colon cancer cells (HCT116), human intestinal fibroblasts and monocytes. The developed MCTS 3D model mimicked several tumor features with cells undergoing spatial organization and producing extracellular matrix, forming a mass of tissue with a necrotic core. Furthermore, monocytes were differentiated into macrophages with an anti-inflammatory, pro-tumor M2-like phenotype. For a combined chemoimmunotherapy effect, spermine-modified acetalated dextran nanoparticles (NPs) loaded with the chemotherapeutic Nutlin-3a (Nut3a) and granulocyte-macrophage colony-stimulating factor (GM-CSF) were produced and tested in 2D cultures and in the MCTS 3D model. NPs were successfully taken-up by the cells in 2D, but in a significant less extent in the 3D model. However, these NPs were able to induce an anti-proliferative effect both in the 2D and in the 3D models. Moreover, Nut3a was able to partially shift the polarization of the macrophages present in the MCTS 3D model towards an anti-tumor M1-like phenotype. Overall, the developed MCTS 3D model showed to recapitulate key features of tumors, while representing a valuable model to assess the effect of combinatorial nano-therapeutic strategies in CRC. In addition, the developed NPs could represent a promising approach for CRC treatment.

Keywords

Nanoparticles; Cancer; Spheroids; Chemoimmunotherapy; Acetalated dextran; Nutlin-3a

1. Introduction

Nowadays, CRC is the third most common and the second deadliest type of cancer worldwide [1]. During its progression, CRC tends to metastasize and, despite the intensive effort to develop efficient and effective diagnosis tools and anticancer therapies [2, 3], its 5-year survival rate is lower than 14% once metastasis occurs [4]. The tumor microenvironment (TME) of CRC is directly associated with the progression of this disease and malignancy [5]. Cancer associated fibroblasts (CAF), one of the main constituents of the TME stroma, play a preponderant role in the tumor, producing ECM and secreting soluble factors (e.g., cytokines), affecting tumor proliferation, cellular migration and immunosuppression [6]. Tumor associated macrophages (TAMs), another major cellular subset of the TME [7, 8], have crucial implications on tumor progression, immunosuppression and ECM remodeling [9]. Macrophages can be polarized towards either M1 (pro-inflammatory and anti-tumor) or M2 (anti-inflammatory and pro-tumor), exhibiting a continuum of phenotypes, which can change upon different stimuli [10, 11]. However, TAMs are mainly M2-like macrophages in the TME and their presence in the cancer tissue is generally linked to poor prognosis. The use of single therapies for CRC has promotes inconsistent benefits, while inducing toxicity [12]. In order to avoid this problem, the use of combinatorial approaches and synergistic tackling of multiple elements in the TME, can promote an enhanced effect of the anticancer therapy, diminishing its side effects and avoiding tumor recurrence [13, 14].

Chemoimmunotherapy is a promising combinatorial approach, which has shown killing effect on cancer [15]. Depending on their mechanism of action, chemotherapeutics can act by inducing tumor cell death in different manners, while simultaneously modulating the immune response. These compounds can possibly induce immunogenic cell death, subvert tumor-induced

immunosuppressive mechanisms, and target/modulate the differentiation and polarization of specific cell subpopulations, such as CAFs and TAMS [15, 16]. The simultaneous use of immunomodulatory molecules (*e.g.*, cytokines, interleukins, and antibodies) with chemotherapeutics can further enhance their impact on the immune system, promoting an antitumor immune response.

The efficiency of this strategy can still be improved using biomaterials, such as nanoparticles (NPs) [17]. NPs represent a powerful tool for drug delivery due to their numerous advantages, such as the ability to encapsulate and protect different payloads, control their release, and deliver them to specific cells. Thereby, the application of combinatorial strategies, such as chemoimmunotherapy based on NPs, has shown improved results in CRC therapy by shifting the paradigm of cancer treatment [13, 18]. Nevertheless, despite showing numerous advantages, the clinical translation of developed NPs for CRC treatment remains limited [13]. One major hurdle is the absence of valuable models capable of predicting the therapeutic outcome in a clinical setting. The most frequently used and well-established models for pre-clinical testing are *in vitro* 2D cell culture models [19, 20]. These models consist of simple cell monolayers that cannot fully mimic the complexity of the TME and recapitulate the myriad of interactions between its different cellular and non-cellular components, known to be critical to cell response and clinical outcome [21]. Hence, despite the use of NPs and different immunotherapy strategies that have shown promising results *in vitro*, the same outcome has not been observed when these reach the clinics. Furthermore, the use of *in vivo* models is hampered by ethical issues and interspecies differences [22]. Thus, it is crucial to develop new models that are able to overcome the aforementioned challenges in the preclinical evaluation of immunity mediated anticancer effect of nanomaterials.

Multicellular tumor spheroids (MCTS) are three dimensional (3D) cellular self-aggregates, which emulate several physiological aspects of human tumors, including the dynamic interplay between the TME constituents [23]. These models can be constituted by a heterogenous cellular population (*e.g.*, tumor cells, fibroblasts and immune cells) [24, 25], producing their own ECM, secreting soluble factors, and changing their genetic profile to a more biologically-relevant state [26]. Furthermore, MCTS tend to have a growth pattern characterized by an exponential volume increment in the earlier stages followed by a growth plateau, which is observed in some solid avascular tumors...[27-29] Moreover, MCTS form a gradient of pH and nutrients, and self-organize into a structure similar to a non-vascularized tumor [23]. Thereby, due to their intrinsic characteristics, MCTS represent a promising approach to screen new developed anticancer therapies, namely those based on nanomaterials, providing results similar to the ones obtained *in vivo* [30].

In this work, a heterotypic MCTS model of CRC was developed to test the efficacy of polymeric NPs co-loaded with a chemotherapeutic drug and a cytokine. The MCTS model was constituted by epithelial colon cancer cells (HCT116), human intestinal fibroblasts (HIF) and human monocytes, which were differentiated mostly into M2-like macrophages. Spermine-modified acetalated dextran (Sp-AcDEX) NPs were loaded with the non-genotoxic drug Nutlin-3a (Nut3a) and the Granulocyte-Macrophage Colony-Stimulating Factor (GM-CSF) that were previously developed by our group [31]. The effect of the nanosystem on the CRC MCTS 3D model was investigated by comparing the cellular association of the developed nanosystem and its ability to induce an anti-proliferative effect in 2D monolayers and in the CRC MCTS 3D model. The ability of the developed nanosystem to polarize the macrophages present in the CRC MCTS model was also assessed.

2. Experimental Section

Materials: All the materials and reagents used in this study are described in the Supporting Information

Ethics Statement: Human samples were obtained in agreement with the principles of the Declaration of Helsinki. Monocytes were isolated from surplus buffy coats from healthy blood donors, kindly provided by the Immunohemotherapy Department of Centro Hospitalar Universitário São João (CHUSJ), Porto, Portugal. Procedures were approved by the Centro Hospitalar Universitário São João Ethics Committee (protocol 90/19). Blood donors provided informed written consent that the byproducts of their blood collections could be used for research purposes.

Synthesis of Spermine-modified Acetalated Dextran: The synthesis of Sp-AcDEX was performed as described elsewhere [32-34].Dextran was first oxidized by stirring a solution of dextran (5 g) and sodium periodate (1.1 g) in MilliQ-water (20 mL) for 5 h at RT. The obtained oxidized dextran was then purified by dialysis in double-distilled water (dd-H_2O) with a regenerated cellulose membrane (Spectra/Por RC tubin MWCO 3.5 kDa). The partially oxidized dextran was lyophilized and purged with N_2 in a dry two neck round-bottom flask. Acetalation of dextran was performed by dissolving dextran (3 g) with anhydrous dimethyl sulfoxide (DMSO, 30 mL) and adding pyridinuim-ptoluenesulfonate (48.6 mg) and 2-methoxypropene (10.6 mL) to the solution. After 1 h reaction time, the reaction was quenched with triethylamine (TEA, 1 mL) and the resulting acetalated dextran precipitated in dd-H_2O (200 mL). AcDEX was collected by centrifugation (20000*g*, 10 min), washed twice with TEA solution (0.01% v/v, pH 8; 100 mL) and dried with vacuum drying (50 °C) for two days. Next, modification with spermine was

performed by dissolving partially oxidized AcDEX (2 g) in DMSO (20 mL), followed by the addition of spermine (4 g). The solution was stirred for 24 h at 50 °C. Afterwards, $NaBH_4$ (1 g) was added and the solution was stirred for 24 h at RT. To dissolve the excess of $NaBH_4$, DMSO (20 mL) and methanol (10 mL) were added to the flask. Finally, Sp-AcDEX was precipitated with MilliQ-water (80 mL), and collected by centrifugation (20000*g*, 10 min). The polymer was washed five times with MilliQ-water (pH 8; 40 mL) by centrifugation and discarding the supernatant. The final product was lyophilized, yielding Sp-AcDEX (1.6 g) as a white powder.

Fabrication of Spermine-modified Acetalated Dextran Nanoparticles: The Sp-AcDEX NPs were prepared by a double emulsion technique (water-in-oil-in-water), as described elsewhere [31, 34, 35]. Sp-AcDEX (12.5 mg) was dissolved in ice cold dichloromethane (DCM, 250 µL). Afterwards, 25 µL of the PBS (pH 7.4) was added dropwise to the polymer solution and the mixture was sonicated in an ice bath. Sonication was performed using a probe sonicator (Vibra-Cell™ ultrasonic processor (Sonics and Materials, Inc., USA) for 30 s of pulsed sonication (10 s ON followed by 5 s OFF), with an amplitude of 50%. Next, PVA 2% (w/v; 500 µL) was added to the first emulsion and the solution was sonicated again in the same conditions. After sonication, the resultant emulsion was poured into a PVA 0.2% solution (w/v; 2.5 mL) and stirred (300 rpm) for 3 h to evaporate the remaining DCM. Finally, the NPs were collected by centrifugation (20000*g*, 5 min, 4 °C) and washed twice with HEPES at pH 8 (500 µL) by centrifugation and removal of the supernatant.

To prepare Nut3a-loaded NPs, Nut3a (400 µg) was dissolved in DCM together with Sp-AcDEX. GM-CSF was loaded by adding GM-CSF solution (25 µL, 5 ng/mL) instead of PBS to prepare the first emulsion.

FITC loaded NPs were prepared by dissolving FITC in DCM before dissolving Sp-AcDEX in the same solution. These NPs were washed six times to ensure the complete removal of free FITC from the NPs surface.

Characterization of the Nanoparticles: NPs average size, PdI and surface charge (ζ-potential) was measured by dynamic light scattering (DLS). Prepared NPs were dispersed in HEPES (pH 7.4, 10×10^{-3} M) before measuring. To assess the association efficiency (AE) of Nut3a, Nut3a-loaded NPs (1.25 mg) were dispersed in DMSO (1 mL) and sonicated in ultrasonic bath (5 min) to promote dissolution of the NPs and Nut3a release. Following completely dissolution of the NPs, the solution was centrifuged (20000*g*, 5 min, 10 °C) and the supernatant collected and analyzed by high performance liquid chromatography (Merck-Hitachi HPLC). All the supernatants from NP preparation and washing were also analyzed. For HPLC quantification, a Symmetry C18 column, 4.6 × 250 mm, 5 µm (Waters, USA) was used. The mobile phase contained 0.1% of trifluoroacetic acid (TFA) (v/v) and acetonitrile (ACN) 0.1% of TFA (v/v) in a ratio of 55:45, respectively, and was set at a flow rate of 1 mL min^{-1}. The detection wavelength was 280 nm.

Cells and Culturing: HCT116 human colorectal cancer cells were obtained from American Type Culture Collection (ATCC, USA). Cells were cultured in Roswell Park Memorial Institute (RPMI)-1640 media, supplemented with 10% of heat inactivated FBS, penicillin (100 IU/mL) and streptomycin (100 mg/mL), and incubated in 5% CO_2 and 95% relative humidity at 37 °C. Subculturing was conducted according to the protocol provided by ATCC. HIF were acquired from ScienceCell™ Research Laboratories (USA). Cells were cultured in Fibroblasts Medium and subcultured according to the protocol provided by the company. Human monocytes were isolated from buffy coats from healthy blood donors using RosetteSep-Human Monocyte

Enrichment Cocktail (StemCell Technologies, France), following the manufacturer's instructions.

Multicellular Tumor Spheroids Formation: MCTS were formed using commercially available micro-molds (3D Petri Dish®, from MicroTissues Inc.). First, agarose (2 %, w/v) was dissolved in NaCl (0.9 %, w/v) and casted in 3D Petri Dish® micro-molds to form molds with 81 homogenous circular recesses. Next, the molds were placed in 12-well plates and RPMI media (2 mL) was added to each well to equilibrate the molds for at least 2 h before cell seeding. Afterwards, cells suspension (190 µL; 2.13 × 10^6 cells/mL), corresponding to *ca*. 5000 total cells per MCTS, were added to the molds and allowed to settle for 30 min, before adding media (2 mL) to each well. Media was replaced every other day.

MCTS were produced in monoculture (HCT116 cells), double culture (HCT116 and HIF) and triple culture (HCT116, HIF and monocytes), keeping the total number of cells per MCTS at 5000 cells. Two different densities, 5000 and 10000 cells per MCTS at day 0 were tested for monoculture MCTS. Also, three different ratios were tested for HCT116:HIF double culture (4:1; 1:1 and 1:4) and one ratio for Monocytes:HCT116:HIF triple culture (4:1:4). When using monocytes, media was supplemented with M-CSF (50 ng/mL) for macrophage differentiation.

Multicellular Tumor Spheroids Size Measurement: At determined time-points (1, 4, 7 and 10 days), MCTS were monitored, and images were taken using a Brightfield microscopy (ZOE™ Fluorescent Cell Imager, Bio-Rad Laboratories). The size was determined by measuring the diameter of the MCTS, using ImageJ software. The average size of each condition was calculated by performing the average of two diameters measurements per MCTS, evaluated in at least nine different MCTS.

Cell Metabolic Activity of Multicellular Tumor Spheroids: The metabolic activity of MCTS was measured overtime with resazurin assay, as described elsewhere.[36] Briefly, at determined timepoints (1, 4, 7 and 10 days), MCTS (≥10 MCTS/condition) were collected from the molds and seeded in in 96-well plates. RPMI containing 20% resazurin (v/v; 300 µL) was added to each well and incubated in the dark at 37 °C for 2 h. Following the incubation, the media was transferred (3 × 100 µL per well) to a 96-well plate with opaque black walls, and the fluorescence was measured at the excitation and emission wavelengths of 530 nm and 590 nm, respectively, using a SynergyMx™ MultiMode Microplate Reader (BioTek™, USA). The obtained fluorescence values were normalized to the number of MCTS per well. All samples were done at least in triplicate.

Multicellular Tumor Spheroids Histological Analysis: At predefined time-points (1, 4, 7 and 10 days), the media was removed from the wells and MCTS were fixed in 4% of PFA (v/v in PBS; 2 mL per mold; 30 min; RT). Afterwards, the molds were washed three times with PBS (2 mL), and either Histogel™ or agarose 1% (w/v) was added to the top of each mold to fix spheroids into the molds. The molds were then embedded in paraffin using an automated embedding system (Thermo Scientific™ STP 120 Spin Tissue Processor). Paraffin embedded samples were sectioned into 3 µm sections, deparaffinized in xylene and rehydrated in graded alcohol series. Staining was performed with H&E.

Immunohistochemistry of Multicellular Tumor Spheroids: Immunohistochemistry was performed as described elsewhere.[36] First, fixed paraffin embedded samples, prepared as described above, were sectioned in 5 µm sections, followed by deparaffinization in xylene and rehydration in sequentially decreasing ethanol concentrations. Before staining, to retrieve the antigens, sections were treated with TE (10×10^{-3} M Tris–1×10^{-3} M EDTA, pH 9) or sodium citrate

buffer (10×10^{-3} M, pH 6), at 96 °C for 30 min. Next, samples were washed three times by immersing sections in PBS (pH 7.4), under agitation (60 rpm) for 5 min. To permeabilize the samples, sections were immersed in triton 0.25% (v/v) at 60 rpm for 10 min and then washed 3 times, as described above. Before adding antibodies, samples were blocked with 10% of FBS in PBS for 1 h at RT. Primary human antibodies (Anti-EpCAM 1:1000, Anti-Vimentin 1:50, Anti-CD68 1:100 and Anti-Fibronectin 1:200) were added to the samples and incubated overnight, in a wet chamber, at 4 °C. Samples were washed three times and the secondary antibodies (at 1:400 dilution) and DAPI solution diluted in 5% of FBS in PBST (v/v) were incubated in a wet chamber, in the dark, for 1 h at RT. Finally, sections were mounted with VectaShield (H-1000, Vector), and imaged with Zeiss AxioImager Z1 microscope (Carl Zeiss, Germany) equipped with an AxioCam MR ver.3.0.

Multicellular Tumor Spheroids Characterization by Flow Cytometry: After 7 days of culturing, MCTS (~40 MCTS per sample) were collected into an Eppendorf tube, centrifuged (400*g*, 5 min, 4°C), and the medium removed. Samples were then washed once with PBS (500 µL) by centrifugation, in the same conditions, followed by removal of the supernatant. MCTS were dissociated to a single cell suspension by incubation with trypsin-EDTA (0.25 %; 300 µL) for 30 min at 37 °C, and by pipetting every 5 min during incubation time. Afterwards, complete media (1 mL) was added to inactivate the trypsin and cells were centrifuged and washed twice with PBS containing 2% of FBS (v/v; 300 µL). Next, cells were resuspended in a solution (100 µL) of PBS containing 2% FBS with the primary antibodies (anti-EpCAM 1:400; anti-CD14 1:50 and anti-CD90 1:140) and incubated (30 min, 4 °C) in the dark. After incubation, cells were washed twice with PBS containing 2% FBS, and resuspended in a solution (100 µL) of PBS 2% FBS with the secondary antibody (1:100) and incubated (30 min, 4 °C) in the dark. Finally, samples

were washed twice, resuspended in PBS containing 2% FBS (300 µL) and filtered through a 70 µm pore filter membrane. Samples were analyzed with BD FACSCanto™ II flow cytometer (BD Biosciences, USA). All data was processed with FlowJo software (Tree Star, Inc., USA). Experiments were performed at least in triplicate.

Nanoparticles Biocompatibility in 2D Cultures: The biocompatibility of the Sp-AcDEX NPs in HCT116, HIF and macrophages was measured by a resazurin-based assay. For HCT116 and HIF, 1×10^4 cells per well were seeded in 96-well plates and allowed to attach overnight. After that, the medium was removed and different concentrations (50, 100, 200 and 500 µg/mL) of NPs suspension in complete medium (100 µL) were added to the cells and incubated for 24 h and 48 h, at 37 °C under 5% CO_2 and 95% of relative humidity. All data was normalized regarding the negative control (complete medium), which was considered 100 % viability. At each time-point, the medium was removed and 100 µL of resazurin 10 % (v/v) in complete media were added to each well and incubated for 2 h at 37 °C in the dark. After, fluorescence was measured at the excitation and emission wavelengths of 530 nm and 590 nm, respectively, using a SynergyMx™ MultiMode Microplate Reader (BioTek™, USA). All samples were done at least in quadruplicate.

To assess the biocompatibility of the macrophages, 1×10^4 monocytes per well were seeded in 96-well plate and incubated for 7 days in RPMI supplemented with 50 ng/mL of M-CSF to allow differentiation into macrophages. After, cells were treated in the same manner as HCT116 and HIF.

Antiproliferative Effect of Nutlin-3a Loaded Nanoparticles and Free Nutlin-3a in 2D Cultures: To assess the anti-proliferative effect of Nut3a-loaded NPs and free Nut3a, a resazurin assay was performed, with the experimental conditions being equal to the ones used for cell viability, as

aforementioned. Here, instead of bare NPs, cells were incubated with either different concentrations of Nut3a-loaded NPs (50, 100, 200 and 500 μg/mL) in complete media or with a range of concentrations of free Nut3a (0 to 120 μM) dissolved in complete media with 1 % of DMSO.

2D Cellular Association: 2D cellular association was assessed in HCT116 cells. Firstly, 1×10^4 cells per well were seeded in 96-well plates and allowed to attach overnight. After that, the medium was removed and FITC loaded NPs suspension in complete medium (50 μg/mL, 100 μL) were added to the cells and incubated for 24 h and 48 h, at 37 °C, under 5% CO_2 and 95% of relative humidity. At each time-point, the medium was removed, and the cells collected and washed twice with PBS. Afterwards, cells were analyzed with BD FACSCanto™ II flow cytometer (BD Biosciences, USA). All data was processed with FlowJo software (Tree Star, Inc., USA). Experiments were performed at least in triplicate.

3D Cellular Association: Triple culture MCTS were cultured for 7 days in 12-well plates, as described above. At day 7, the medium was removed from the wells and FITC loaded NPs dispersed in complete media (200 μg/mL, 2 mL) were added to each well and incubated for 24 and 48 h at 37 °C under 5% CO_2 and 95% of relative humidity, and under agitation on an orbital shaker at 50 rpm. After that, MCTS (*ca*. 80 spheroids/sample) were collected to Eppendorf tubes, dissociated to single cell suspension, as previously explained, and washed twice with PBS. Samples were resuspended in PBS containing 2 % of FBS and filtered through a 70 μm pore filter membrane and analyzed with BD FACSCanto™ II flow cytometer (BD Biosciences, USA). All data was processed with FlowJo software (Tree Star, Inc., USA). Experiments were performed at least in triplicate.

Nanoparticles Biocompatibility in 3D Cultures: The biocompatibility of Sp-AcDEX NPs on MCTS was evaluated by measuring the ATP content of the cells, which is directly proportional to the number of viable cells in culture [37]. First, triple culture MCTS were cultured for 7 days in 12-well plates, as described above. At day 7, spheroids were collected and seeded (1 to 3 spheroids per well) in complete media (100 µL) in Corning® spheroid microplates with 96-wells. After that, 100 µL of different concentrations of NPs suspension in complete media (100, 200, 400 and 1000 µg/mL) were added to each well and incubated at 37 °C, under agitation (30 rpm) for 24 h and 48 h. At each time-point, 100 µL of medium was removed and 100 µL of CellTiter-Glo® 3D Reagent (Promega Corporation, USA) were added. Plates were shaken (100 rpm) for 5 min and incubated for 25 min at RT. Luminescence was measured using a SynergyMx™ MultiMode Microplate Reader (BioTek™, USA). All samples were performed at least in quadruplicates.

Antiproliferative Effect in 3D Cultures: To test the anti-proliferative effect of the Nut3a-loaded NPs and free Nut3a in MCTS, a similar study to biocompatibility study was performed. Here, instead of bare NPs, 100 µL of Nut3a-loaded NPs dispersed in complete media (100, 200, 400 and 1000 µg/mL) and free Nut3a dissolved in complete media with 1 % of DMSO (10, 20, 40, 80, 160 µM) were incubated with MCTS. Viability was assessed by ATP measurements, as described above.

Macrophage Polarization: Triple culture MCTS were cultured for 7 days in 12-well plates. At day 7, the medium was removed from the wells and bare NPs and Nut3a NPS dispersed in complete media (200 µg/mL, 2 mL), free Nut3a (10 µM, 2 mL) and free GM-CSF (2 ng/mL, 2 mL) were added to each well and incubated for 48 h at 37 °C under 5% CO_2, 95% of relative humidity, and under agitation on an orbital shaker at 50 rpm. After, MCTS (*ca*. 80 spheroids per

sample) were collected to Eppendorf tubes, dissociated to single cell suspension, as explained above, and washed twice with PBS. Next, cells were resuspended in a solution (100 µL) of PBS containing 2 % of FBS with anti-CD14 (1:50), anti-CD86 (1:50) and anti-CD163 (1:25) antibodies and incubated (30 min, 4 °C) in the dark. After incubation, cells were washed twice with PBS containing 2% FBS, resuspended in PBS containing 2% FBS (300 µL) and filtered through a 70 µm pore filter membrane. Samples were analyzed with BD FACSCanto™ II flow cytometer (BD Biosciences, USA). All data was processed with FlowJo software (Tree Star, Inc., USA). Experiments were performed at least in triplicate.

Statistical Analysis: Results are expressed as mean ± standard deviation (s.d.) of at least three independent experiments. Statistical significance was analyzed with two-way analysis of variance (ANOVA) with Bonferroni test, with the level of significance set at probabilities of $*p < 0.05$, $**p < 0.01$, $***p < 0.001$ and $****p < 0.0001$. All statistical analyses were performed using GraphPad Prism (GraphPad Software, San Diego, CA).

3. Results and Discussion

3.1. Optimization and Characterization of a Heterotypic Triple Culture MCTS model

One of the major goals of this work was to develop a 3D heterotypic *in vitro* model, capable of closer recapitulating the TME, providing a platform to assess the efficacy of nanomaterials designed for chemoimmunotherapy. The co-culture of tumor cells with fibroblasts and monocytes in MCTS was prepared to reproduce the 3D structure of tumors and the intrinsic interactions between the ECM and different cell types, which are known to affect disease progression and the efficacy of anticancer therapies [38-40].

To develop this heterotypic triple model, microwell array technology [36, 41-43] was employed (Scheme 1). In this technique, cells are seeded in microwells composed of non-adhesive hydrophilic hydrogels which inhibit cell-surface interactions, thus promoting cell–cell interactions and aggregation, leading to the formation of spheroids [44]. With commercially available microwell arrays it is possible to simultaneously produce multiple spheroids in a high-throughput fashion. Here, cells were seeded in agarose micro-molds produced with 3D Petri Dish®, and the formation and characteristics of MCTS were analyzed overtime.

In order to optimize the triple culture MCTS and choose the best culture conditions for their formation, we had to study the impact of each cell line in their characteristics. Thus, we have firstly prepared and characterized monoculture HCT116–MCTS, followed by the gradual addition of fibroblasts and monocytes.

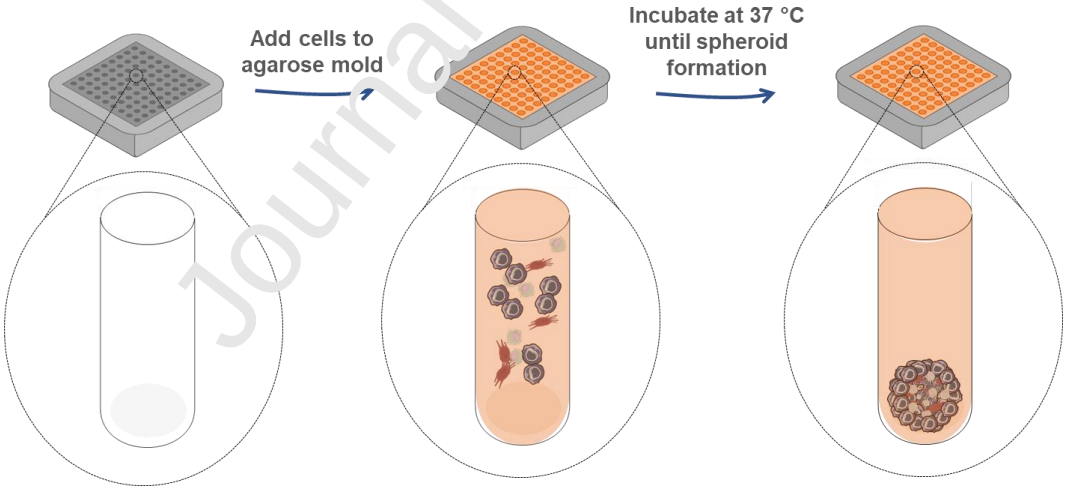

Scheme 1. Schematic representation of MCTS formation by liquid overlay technique, using agarose molds. Image generated with medical art servier.

3.1.1. Monoculture MCTS:

To produce monoculture of HCT116 MCTS, two different cell densities (5000 and 10000 cells per MCTS) were seeded on agarose micro-molds, and MCTS morphology and size, along with cell metabolic activity and production of ECM were assessed along 10 days (**Error! Reference source not found.**). As observed by brightfield microscopy (**Error! Reference source not found.**A), at day one (D1), irregular and loose cell aggregates were formed at all initial cell densities. Yet, the morphology of these aggregates changed overtime into spherical and more compact MCTS. The analysis of MCTS diameter (**Error! Reference source not found.**B) demonstrated a size reduction of approximately 80 µm from D1 to D4, followed by a steady growth rate up to D10, which is consistent with the slow proliferation rate observed in compact tissue structures [45]. At D10, regardless of the initial cell density, all MCTS reached a similar average size of 520 µm. Their metabolic activity was measured overtime through a resazurin-based assay (**Error! Reference source not found.**B), and nearly constant levels were maintained along 10 days of culture, which are in agreement with the typical steady growth rate of MCTS. Additionally, histological analysis of MCTS morphology was performed by hematoxylin and eosin (H&E) staining (**Error! Reference source not found.**C). The H&E staining's corroborated the formation of loose cell aggregates at D1, and the higher cellular organization in MCTS at D4. Furthermore, after 7 days of culturing, the MCTS developed a necrotic core as seen by the presence of condensed chromatin and nuclear disintegration [46, 47] (Figure 1C). The development of necrotic cores is typical for spheroids with diameter over 400–500 µm, as the high compaction of such structures promotes the creation of a gradient of nutrients and oxygen, with formation of a hypoxic core with dead cells. Additionally, quiescent, viable and proliferative cells are usually located in the outer rim of the spheroids[48-51]. Here, the presence of proliferative and apoptotic cells was analyzed by Ki67 and Caspase 3 staining,

respectively (Figure S1). As expected, cells in the outer layer of the spheroid were highly proliferative (stained Ki67 positive), and only low amounts of apoptotic cells were observed.

The increase in necrotic and quiescent cells, coupled with the decrease in proliferative and viable cells along time, contributes to the low spheroid growth [48]. Additionally, the expression of ECM was analyzed by fibronectin (FN) staining (Figure S2). As seen, these MCTS were only able to synthesize low amounts of ECM, as suggested by the low fibronectin (FN) expression(Figure S2). Considering these results, as there were no major differences in spheroid formation and characteristics between the tested initial cell densities, we opted to fix the density of 5000 cells per spheroid in subsequent studies. Furthermore, as we wanted a spheroid model with a necrotic core, in order to represent a more advanced tumor stage, seven days of spheroids culturing was considered as the optimal condition to be used in all further experiments.

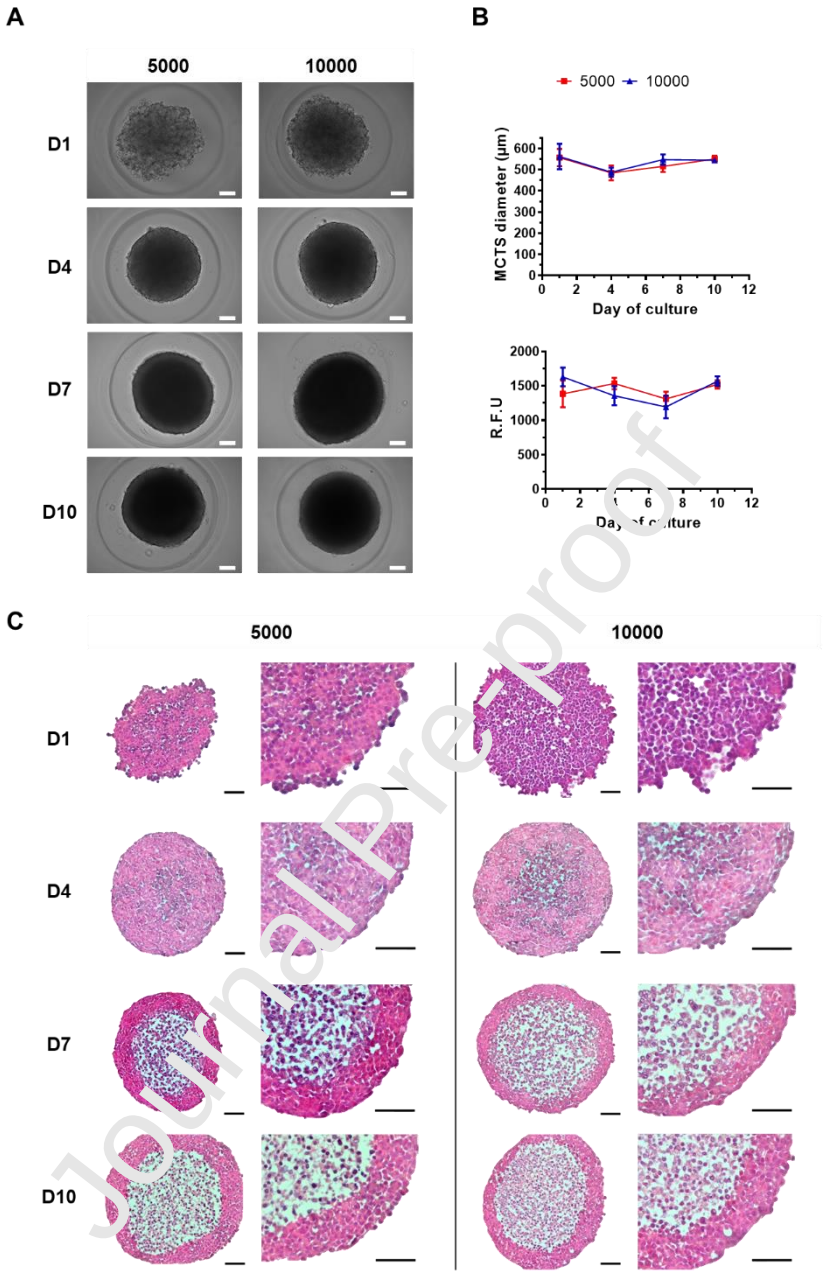

Figure 1. HCT116 monoculture MCTS formation and characterization along ten days. A) Over time brightfield microscopy images of the morphology of MCTS with two different initial cultured cell densisites. Scale bar represents 100 µm. B) MCTS diameter and metabolic activity evolution over time as function of initial seeding cell density. Values represent mean ± s.d.($n \geq 3$) C) H&E staining of the different formed MCTS (and respective magnification, portrayed on the right). Scale bar represents 100 µm.

3.1.2. Double culture MCTS

Fibroblasts are one of the main constituents of the TME, playing a preponderant role in the production and remodulation of the ECM and highly affecting cell–cell and cell–matrix interactions [52, 53]. Moreover, these cells are involved in assisting several cancer cell activities, promoting cancer progression and metastasis [54, 55]. Thereby, in order to produce a 3D *in vitro* model capable of better recapitulating a solid tumor, it is important to include fibroblasts in its structure. Thus, in the following step, MCTS containing HCT116 cells and human intestinal fibroblasts (HIF) were produced. While keeping the total number of initial cells per spheroid at 5000, two different ratios of HCT116 cells to HIF (1:1 and 1:4) were seeded and culture as prolonged for 7 days. Similar to monoculture, the double culture MCTS with 1:1 ratio (Figure 2) formed loose and irregular aggregates at D1, which became more spherical and compact with time (Figure 2A). However, MCTS with higher fibroblasts ratio (1:4 ratio of HCT116 cells to HIF), formed spherical and compact structures at D1. Furthermore, a correlation between the ratio of cells and the MCTS diameter was observed, with MCTS containing higher amount of fibroblasts having a smaller average diameter (Figure 2B). Irrespective of the cell ratio, all the MCTS presented a similar average size of 450 µm after 7 days. Also, the metabolic activity profile (Figure 2B) followed a similar trend, with MCTS with less tumor cells showing lower activity levels at D1, but with tendency to reach similar activity levels overtime. As seen in Figure 2Cand Figure 3, the spatial organization of MCTS altered overtime, with fibroblasts (elongated cells, staining positively for vimentin) being localized in the core of the spheroid, surrounded by the HCT116 epithelial tumor cells (positively stained with epithelial cell adhesion molecule, EpCAM). A necrotic core was also formed after 7 days, (Figure 2C and S1). The

synthesis of endogenous ECM was assessed through immunohistochemical analysis of FN expression that, in CRC, was found to be expressed in tumor ECM, but not in healthy tissue [56]. FN deposition was directly correlated with the presence of fibroblasts, since MCTS with HIF evidenced higher FN deposition than the monoculture ones (Figure 3 and Figure S2). In addition, since fibroblasts and ECM are key constituents of the TME, the ratio of 1:4 was selected as the optimal condition for subsequent studies.

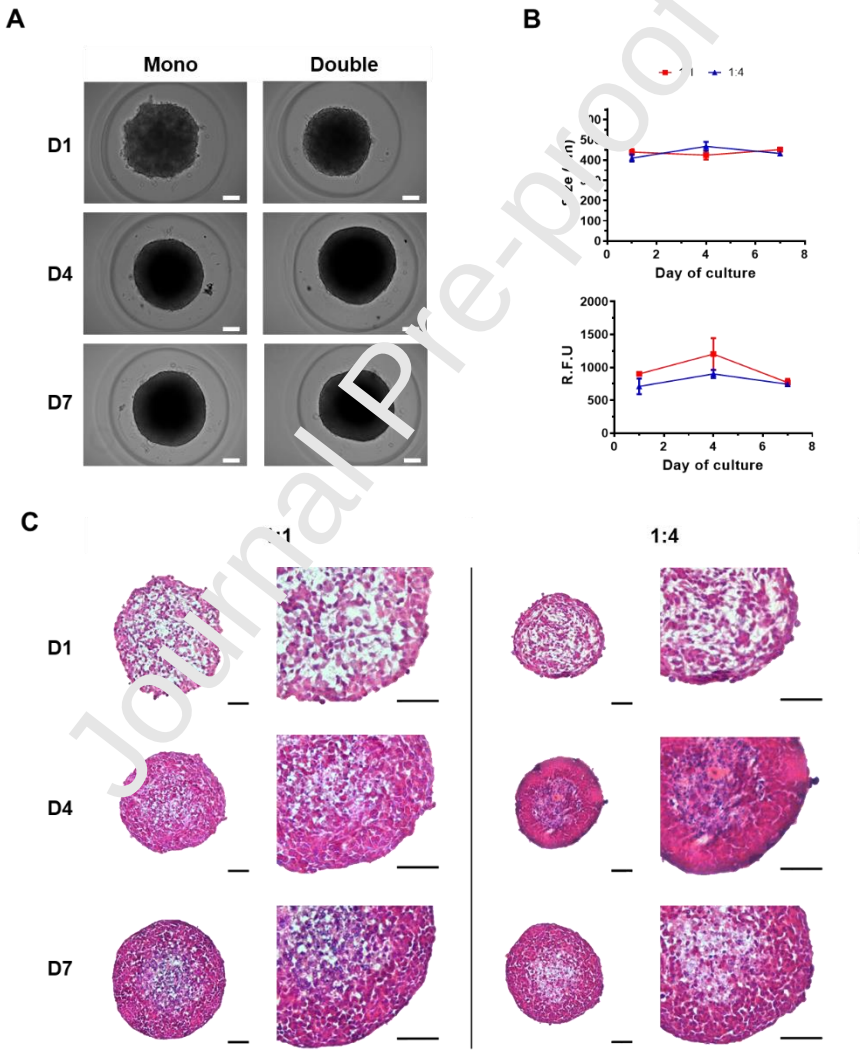

Figure 2. Characterization of HCT116:HIF co-culture MCTS. A) Over time brightfield microscopy images of the morphology of MCTS with two different tumor cells to human

instentinal fibroblasts ratios. Scale bar represents 100 µm. B) MCTS diameter and metabolic activity evolution along seven days as function of initial seeding cell density. Values represent mean ± s.d. (n ≥ 3). C) H&E staining of the different formed MCTS (and respective magnification, portrayed on the right). Scale bar represents 100 µm

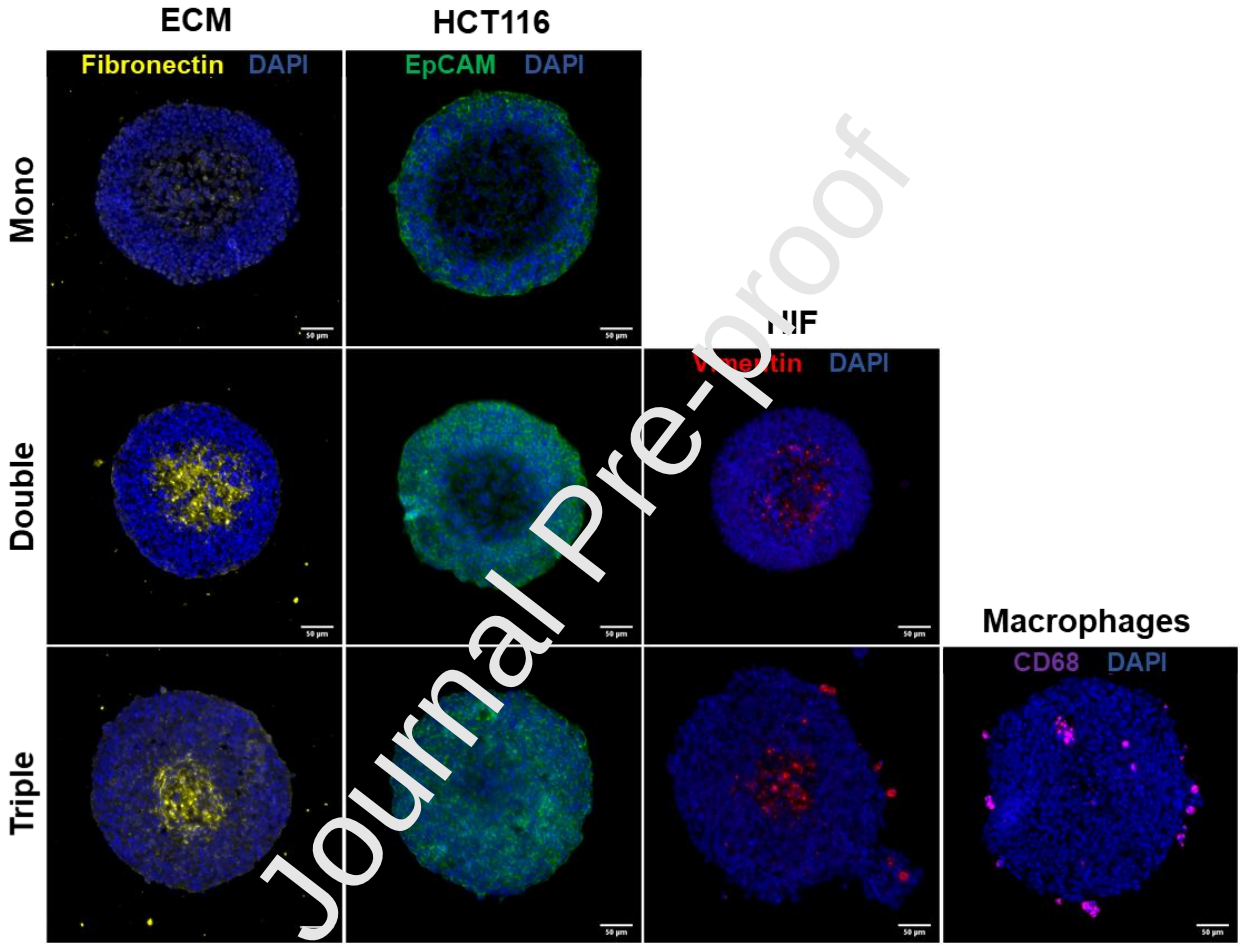

Figure 3. Immunofluorescence microscopy images of D7 mono, double and triple co-culture MCTS. Representative images of cellular organization within the MCTS: FN (yellow); HCT116–EpCAM (green); HIF–vimentin (red); macrophages–CD68 (violet) counterstained with DAPI (blue). Scale bars are 50 µm. (Images for the fibronectin expression are the same as the ones used in Figure S2)

3.1.3. Triple culture MCTS

TAMs are another important subset of cells in the TME that are involved in the CRC progression [57, 58]. These immune cells can be found within or near the tumor tissue, and have been associated to poor clinical prognosis [59]. TAMs originate either from tissue-resident macrophages or from circulating monocytes that upon recruitment, infiltrate into the tumor tissue, and subsequently differentiate into M2 macrophages in response to different stimuli from the TME [60]. Thus, the last step in production of CRC−MCTS was the co-culturing of epithelial tumor cells and fibroblasts with monocytes/macrophages. For this purpose, we have opted to use peripheral blood-derived human primary monocytes to increase the fidelity of the developed model for pre-clinical testing.

Thereby, freshly isolated monocytes were seeded together with HCT116 and HIF cells at a ratio of 4:1:4, respectively, keeping the total number of viable cells seeded per spheroid at 5000. The MCTS were cultured for 7 days and characterized as previously. Additionally, in order to promote the differentiation of monocytes to macrophages, the medium was supplemented with 50 ng/ml of macrophage colony stimulating factor (M-CSF).

As can be observed in Figure 4A, the seeded cells formed compact and spherical MCTS, similar to the double co-culture MCTS. However, unlike to the other conditions, in the triple culture, small cellular aggregates were found on the vicinity of the MCTS, likely corresponding to monocytes which did not penetrate into the MCTS. The diameter of the MCTS increased at a constant rate of around 50 µm every three days (Figure 4B), reaching the same size of double culture MCTS after 7 days. The metabolic activity profile was also increased overtime.

Histological analysis (Figure 4C) showed an identical evolution of the spatial conformation of the triple co-culture MCTS with HIF being located at the core and the HCT116 epithelial cells

being located around them. Furthermore, there was ECM deposition in the core after 4 days of culturing, and the formation of a necrotic core after 7 days. Comparing to the mono and double culture MCTS, the introduction of monocytes in MCTS constitution resulted in some loss of ECM after 7 days, creating an apparently looser structure. According to the literature, TAMs can produce proteolytic enzymes capable of digesting the ECM, which further facilitates cancer migration and dissemination [61, 62].

The spatial distribution of the three cell types at D7 was further investigated by immunofluorescence microscopy (**Error! Reference source not found.**), which confirmed the location of HIF and HCT116 epithelial cancer cells. Macrophage location was assessed by CD68 staining, a highly expressed marker in tissue macrophages. While most of macrophages were found to be around the MCTS, some could penetrate deeply in the MCTS. This data is in accordance with recent published data, showing that $CD68^+$ macrophages are usually located in the tumor invasive front area and there is low accumulation intratumorally [63, 64]. As previously stated, monocytes and macrophages are recruited by different factors from the TME [60]. For example, fibroblasts have shown to secrete cytokines and chemokines that promote the recruitment and adhesion of monocytes and promote their differentiation towards M2 macrophages [58]. Similar to double co-culture MCTS, deposition of FN in the core of the triple co-culture MCTS was also observed (Figure 3).

To further assess the cellular constitution of the triple co-culture MCTS after 7 days in culture, the MCTS were disaggregated and the percentage (%) of each cell type was calculated by flow cytometry. HCT116 epithelial cancer cells constituted the majority of MCTS cells (90.8±2.4 %), while the fibroblasts and macrophages altogether (HIF: 5.6±1.6 %; macrophages: 7.5±1.2%) only represented around 13 % of the cell population. The huge disparity in comparison with the

initial seeded cell ratios is attributed to the non-proliferative nature of the macrophages and the faster proliferation and higher resistance of tumor cells in comparison with fibroblasts.

Taking all results in consideration, the triple co-culture MCTS at D7 was chosen as a viable model to represent an avascular tumor CRC microenvironment.

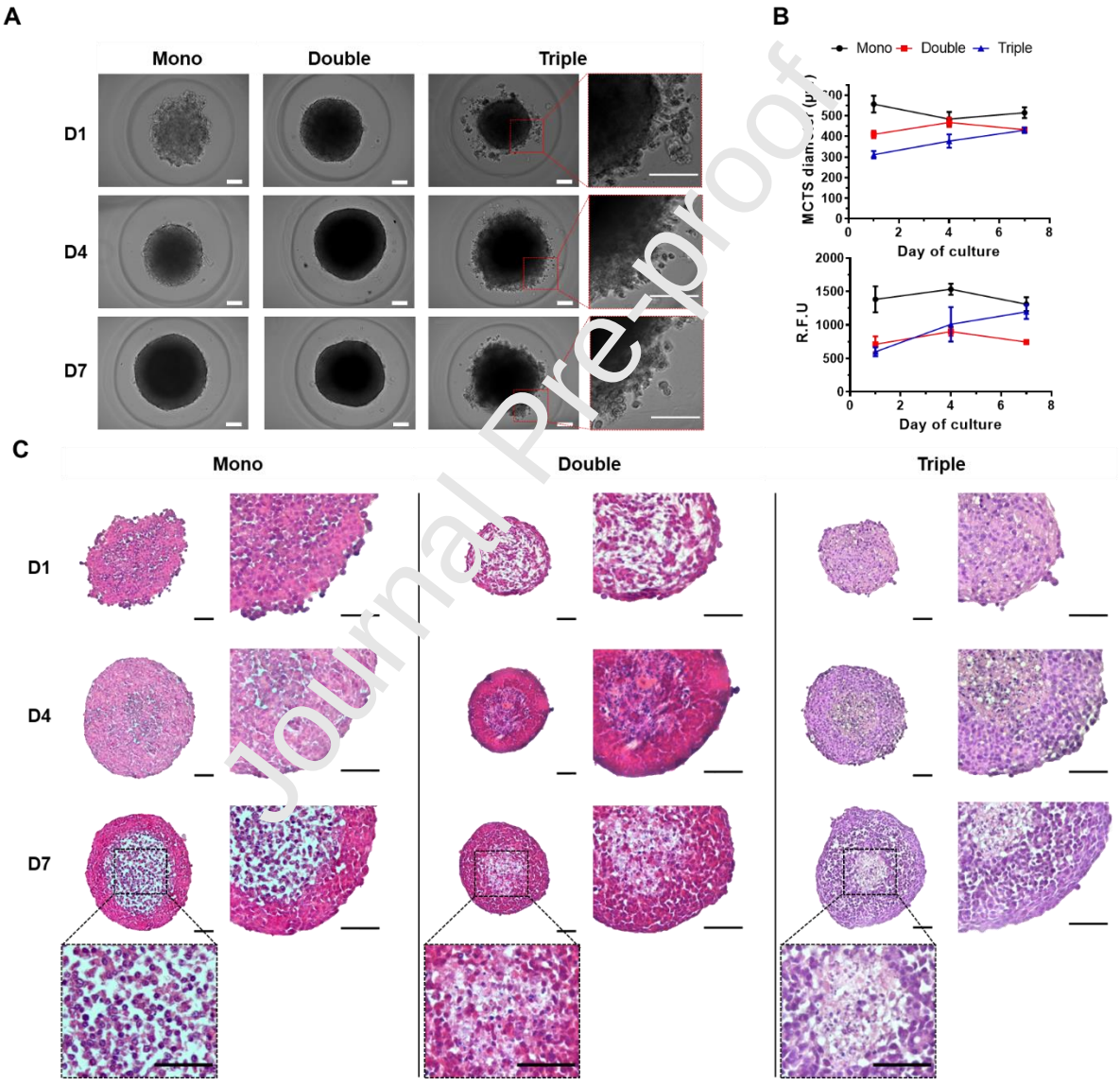

Figure 4. Comparison between mono, double and triple co-culture MCTS. Images for the mono and double culture are the same as the ones used in Figure 1 for 5000 cell density and on Figure

2 for ratio 1:4, respectively. A) Over time brightfield microscopy images of the morphology of the mono, double and triple co-culture. Ampliation of brightfield images of the triple co-culture spheroids at D1, D4 and D7, in order to better observe the cellular aggregates in the vicinity of the spheroid. Scale bars represent 100 µm. Scale bar represents 100 µm. B) MCTS diameter and metabolic activity evolution along 7 days. Values represent mean ± s.d. ($n \geq 3$) C) H&E staining of the different MCTS (and respective magnification, portrayed on the right). Ampliation of sections of mono, double and triple culture spheroids at D7, to observe the core of the spheroid. Scale bar represents 100 µm.

3.2. Nanoparticles Production and Characterization

In this study, polymeric NPs of Sp-AcDEX were prepared by a water-in-oil-in-water double emulsion technique, as previously described by our group [31, 65]. The rationale behind the use of these specific NPs for a chemoimmunotherapy strategy derives from their advantageous characteristics, such as: (i) the ability to encapsulate both hydrophobic and hydrophilic molecules, allowing the conjugation of chemotherapeutics and immunomodulators, as Nut3a and GM-CSF; (ii) intrinsic immunoadjuvant properties; and (iii) ability to control the release of its payloads only upon contact with acidic environment due to the pH-sensitive nature of the polymer [31, 66].

The physicochemical characteristics of the prepared Sp-AcDEX NPs were analyzed by DLS and laser Doppler electrophoresis, and are summarized in Table 1. All the prepared Sp-AcDEX NPs had low PdI values, ranging between 0.10 and 0.19, which indicate a relative homogenous size distribution. Their Z-average ranged between 200 to 230 nm. Due to the polycationic properties of Sp-AcDEX, owing to the presence of amines [34], all Sp-AcDEX NPs presented highly

positive surface charge (ζ-potential) with *ca*. +40 mV. The encapsulation of the different payloads, Nut3a, GM-CSF and FITC, did not significantly impact the physicochemical properties of the NPs. The observed difference on the ζ-potential of FITC NPs compared to the bare NPs in Table 3 is attributed to the use of a different batch of polymer to produce FITC NPs. However, when compared to bare NPs produced from the same batch, no differences in size, PdI and ζ-potential were observed (data not shown).

Table 1. Physicochemical characterization of the bare and loaded 6p-AcDEX NPs used in this study. Values represent mean ± s.d. (n=3)

Samples	Z-Average [nm]	PdI	ζ-potential [mV]	EE [%] Nutlin-3a
Bare NPs	229±2	0.19±0.01	38±2	–
Nut3a NPs	198±1	0.10±0.02	48±2	84±2
GM-CSF NPs	208±1	0.14±0.02	41±3	–
Co-loaded NPs	203±2	0.11±0.01	45±1	86±3
FITC NPs	225±1	0.19±0.03	29±1	–

3.3. Cellular Interaction

One crucial aspect necessary to take into consideration when developing NPs for anticancer strategies is the ability of the NPs to be taken-up by the tumor cells. Commonly, cellular interactions of the developed nanomaterials are assessed in 2D culture monolayers *in vitro*, which lack critical components of the tumor environment. For example, the absence of ECM, which creates a physical barrier and diffusion gradient in the tissue that restricts NPs penetration, greatly impacts the cellular interactions and the reliability of the final results [67-69]. Thereby,

the use of 3D models that can recapitulate several aspects of the TME is becoming more relevant in pre-clinical testing, to obtain better predictive results and facilitate clinical translation[70].

Taking this into consideration, we have evaluated the interaction of the developed Sp-AcDEX NPs in both a 2D monolayer and on the developed triple co-culture MCTS. Since the developed 3D model is mostly constituted of HCT116 epithelial cancer cells, and these cells form the outer layer of the spheroid (**Error! Reference source not found.**) where NPs will be in contact at first, the tested 2D monolayer was also made of HCT116 cells. FITC-labelled NPs were incubated with the 2D model and the triple co-culture MCTS for 24 h and 48 h. At each time-point, the cells were collected, and the fluorescence intensity was measured by flow cytometry. As seen in Figure 5, after 24 h, in the 2D model, *ca*. 88% of the cells were associated with FITC-labelled NPs. Unlike in the MCTS, only a reduced number of cells, *ca*. 26%, were associated with the NPs. After 48 h, a slight decrease of 3% in the 2D model and a small increase in the 3D model to around 29% was observed. The significant difference in the cellular association between the 2D and 3D model can be explained by the conformation of the 3D model, in which the cells are tightly packed and have ECM surrounding them, mimicking more closely an organotypic structure. Thus, while in 2D monolayer, every cell is in direct contact with the FITC-labelled NPs, in the MCTS, the FITC-labelled NPs only have direct contact with the external layer of cells. Thus, the interaction of the FITC-labelled NPs with the cells in the deeper layers is dependent on the ability of the NPs to penetrate into the MCTS. It is known that the physicochemical characteristics of NPs can highly affect their penetration within MCTS. For example, NPs larger than 100 nm have shown limited penetration in MCTS, accumulating preferentially in the periphery [71, 72]. Additionally, the presence of amines and positive surface charge also leads to the accumulation of NPs in the periphery of MCTS and reduction of

penetration [72]. Thereby, we hypothesized that Sp-AcDEX NPs, due to their physicochemical characteristics, accumulate in the periphery of the MCTS, having low penetration. Although this result might look undesirable, several studies have shown that despite these physicochemical characteristics impeding tumor penetration, they promote tumor accumulation, leading to a higher anticancer efficacy of drug loaded NPs [30, 73]. Moreover, the mean fluorescence intensity (MFI) values were similar in both the 2D and 3D cell models, showing a similar interaction between the FITC-labelled NPs and the cells in both models.

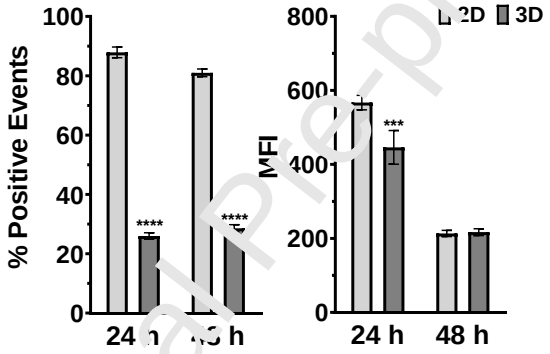

Figure 5. Comparison of cellular association in 2D and 3D cell models of FITC-labelled NPs by flow cytometry. FITC-labelled NPs were incubated for 24 h and 48 h. Samples were analyzed with two-way ANOVA, followed by Bonferroni's post-test. Error bars represent mean ± s.d. ($n \geq 3$).

3.4. Biocompatibility of Sp-AcDEX NPs

To ensure the safety of the developed Sp-AcDEX NPs, their biocompatibility was evaluated in both 2D monolayers and in the developed triple co-culture MCTS. The monolayers were constituted of HIF, macrophages and HCT116 cells. Four different concentrations of bare NPs (50, 100, 200 and 500 µg/mL) were incubated for 24 h and 48 h with the different cell lines, and

cell viability was measured at each time-point (Figure 6). As for the 2D models, the NPs showed a high safety profile up to 48 h in both HIF and HCT116 cells, with viability values above 80% for all tested concentrations. However, the same was not observed for macrophages as, for these cells, a dose and time-dependent cytotoxicity occurred. Sp-AcDEX NPs only presented a safety profile up to 100 µg/mL in the first 24 h, and up to 50 µg/mL after 48 h. It is hypothesized that this higher cytotoxic profile originates from a higher uptake of NPs by macrophages, due to their phagocytic nature [74, 75]. Moreover, macrophages express dextran-binding-C-type lectins and scavenger receptors, which enhance the uptake of dextran NPs [76-78]. Unlike the other tested cells, macrophages derived from human monocytes do not proliferate. Thus, despite the tested NPs concentration being the same, there was a high number of NPs per cell, which might explain higher sensitivity of these cells to the NPs [75]. When analyzing the biocompatibility in the triple co-culture MCTS, all tested concentrations were non-toxic in the first 24 h. After 48 h, a dose and time-dependent toxicity was however observed, with viability values being above 70% up to NPs concentrations of 200 µg/mL.

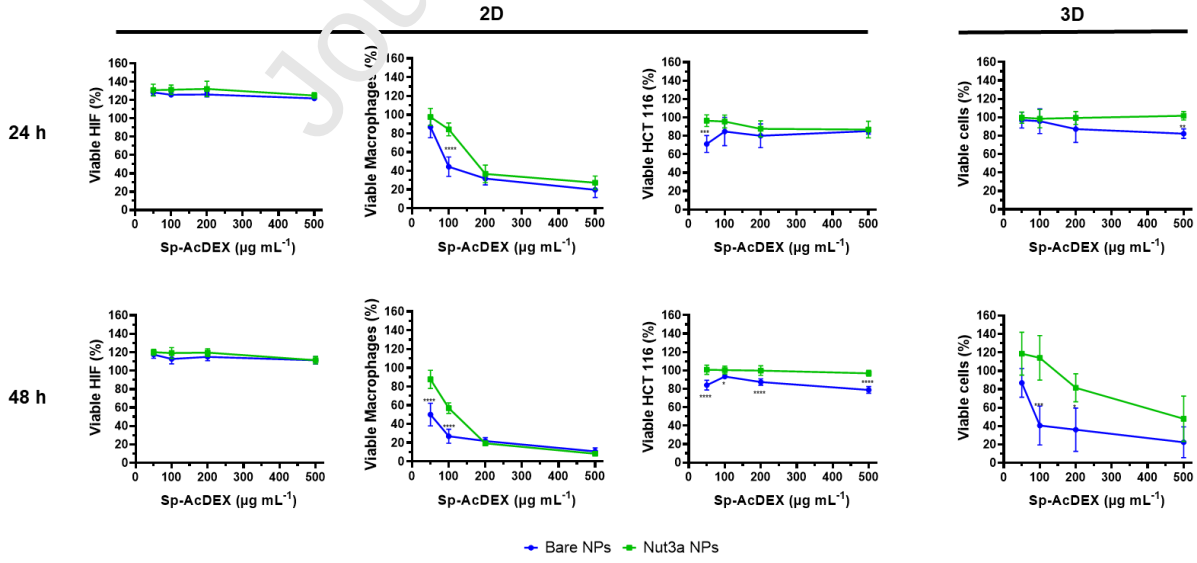

Figure 6. *In vitro* cytotoxicity of Nut3a-loaded NPs by comparison with bare NPs. Bare and Nut3a-loaded NPs (50, 100, 200 and 500 μg/mL) were incubated with HIF, macrophages, HCT116 cells and triple co-culture MCTS for 24 h and 48 h. At each time point, the viability was measured by a resazurin-based assay (in the 2D models) and by measuring the adenosine triphosphate (in the 3D model). All the samples were compared with respective negative control. Samples were analyzed with two-way ANOVA, followed by Bonferroni's post-test. All Results represent mean ± s.d. ($n \geq 4$).

3.5. Antiproliferative Effect of Nut3a-Loaded NPs

The p53 is a gene capable of regulating the cell cycle, inducing cell cycle arrest, apoptosis or senescence upon cellular stress. Thereby, it acts as a tumor suppressor gene, not allowing the proliferation of damaged cells [79-81]. In several types of cancer, p53 function plays a preponderant role in CRC development and progression, since its function is impaired by mutations or overexpression of inhibitors [79, 82]. Several compounds with ability to restore p53 function have been investigated for CRC treatment. For example, Nut3a is a small molecule that acts by inhibiting the p53 proteasomal degradation through the ubiquitin protein ligase murine double minute 2 (MDM2) [83]. By acting as a MDM2 antagonist, Nut3a stabilizes and activates p53 in CRC cells carrying wild type (wt) p53, promoting tumor growth arrest [79, 84]. Furthermore, this compound does not cause DNA damage, which grants its advantage over other chemotherapeutics agents, being a potential therapeutic agent for CRC [84].

To assess the potential of Nut3a-loaded NPs for CRC treatment, we have performed a similar study as for the assessment of the biocompatibility of the NPs. Here, 2D culture monolayers and the triple co-culture MCTS of HCT116 cells (wtp53), HIF and macrophages were incubated with

different concentrations of bare NPs, Nut3a-loaded NPs (50, 100, 200 and 500 µg/mL) and free Nut3a (1 to 100 µM) for 24 h and 48 h, and their viability was checked at each time-point (Figure 6 and S5). The half maximal inhibitory concentration (IC_{50}) values were also calculated (Table 2). Considering the Nut3a association efficiency of 86%, 50, 100, 200 and 500 µg/mL of Nut3a-loaded NPs corresponded *ca*. to 2.4, 4.7, 9.4 and 23.5 µM of Nut3a.

As shown in Figure 6, no toxicity was observed in HIF for all tested concentrations of bare and Nut3a-loaded NPs for up to 48 h. For the same cells, a dose and time-dependent toxicity was observed for free Nut3a (Figure S3), with the IC_{50} values of 48.3 and 29.5 µM after 24 and 48 h, respectively. Nut3a was shown to induce cellular senescence in fibroblasts, thereby suppressing cancer growth [85, 86]. The observed difference between Nut3a-loaded NPs and free Nut3a might be attributed to the fact that, while free Nut3a is already soluble in the media, when encapsulated in the NPs it will only be released upon degradation of the polymer by contact with a more acidic pH [31].

In macrophages, up to 100 µg/mL of both bare and Nut3a-loaded NPs, Nut3a-loaded NPs showed a higher inhibition of cell growth than bare NPs with viability values decreasing from *ca*. 85% to 45% after 24 h and from *ca*. 56% to 26% after 48 h (Figure 6). Moreover, free Nut3a only exerted toxicity for concentrations above 20 µM, and no time-dependent toxicity was observed (Figure S3).

When assessed in HCT116 cells, both Nut3a-loaded NPs and free Nut3a exerted a time and dose-dependent anti-proliferative effect. In the first 24 h, there was no observable reduction in viability values for the tested concentrations of Nut3a-loaded NPs, and only high concentrations of free Nut3a (>20 µM) could induce growth arrest, with IC_{50} value of 53.5 µM. After 48 h, Nut3a-loaded NPs reduced the cell viability in a dose dependent manner, with cell viability

values reducing *ca*. 20% for the highest tested concentration, when compared with bare NPs in the same concentration. Furthermore, free Nut3a exerted a more pronounced dose-dependent effect, reaching an IC_{50} of 16.8 μM. HCT116 cell line, due to its wtp53, was proven to be susceptible to Nut3a treatment [84, 87, 88].

Both Nut3a-loaded NPs and free Nut3a have successfully reduced the cell viability of the triple co-culture MCTS in a time- and dose-dependent manner (Figure 6 and S5). After 24 h of incubation, Nut3a-loaded NPs induced a low inhibition effect, with only the concentrations of 200 and 500 μg/mL capable of reducing the cell viability by 12% and 15%, respectively, compared to bare NPs. Yet, after 48 h, a more pronounced effect was observed, with the viability values ranging from 87% to 22%. Furthermore, Nut3a-loaded NPs had a higher anti-proliferative effect than free Nut3a in MCTS. This enhanced anti-proliferative effect was observed when Nut3a was loaded in NPs, possibly due to the higher accumulation of drug in the MCTS, leading to a higher anticancer efficacy [30, 73].

Although HCT116 cells in 2D culture monolayer were more sensitive to free Nut3a than the triple co-culture MCTS after 48 h (Figure S3), the same finding was not observed when Nut3a was loaded in Sp-ACDEX NPs (Figure 6). While unexpected, due to a significant lower cellular association of the NPs in the MCTS compared to HCT116 2D monolayer (Figure 5), several hypothesis can explain this phenomena. One hypothesis might come from the fact that Sp-AcDEX NPs are pH sensitive and their payload releases only at acidic pH [31, 33, 89]. Thereby, since 3D models, unlike the 2D monolayers, recapitulate the creation of an acidic TME, it is possible that Nut3a is released faster from the NPs in the MCTS than in 2D culture model. Other explanation can possibly come from the inhibition of α5 integrin by Nut3a [90]. The α5β1 integrin is a FN receptor, highly expressed in HCT116 [91], which increases during CRC

progression and under hypoxia, enhancing cell adhesion to ECM and promoting cell proliferation and metastasis [90, 92]. Furthermore, it was shown that Nut3a, by activating p53, decreases the expression of α5 integrin and leads to HCT116 apoptosis [90]. Thus, due to the constitution of the developed MCTS, which contain HCT116, HIF and FN in its ECM, it is possible that when delivering Nut3a to the MCTS, this molecule is also acting through α5 integrin inhibition, leading to an enhanced anti-proliferative effect. However, further studies are needed to unveil the underlying mechanisms behind this augmented response in 3D comparatively to 2D models. Nonetheless, these results show the potential of Nut3a NPs to be used for CRC treatment.

Table 2. Nut3a IC_{50} values after 24 h and 48 h incubation with HIF, macrophages, HCT116 cells and triple co-culture MCTS.

Cells	Nut3a IC_{50} (μM)	
	24 h	**48 h**
HIF	48.3	29.5
Macrophages	38.5	39.1
HCT116	53.5	16.8
Triple co-culture MCTS	32.8	21.0

3.6. Macrophage Polarization

Due to the importance of TAMs in the TME and their "plasticity", TAMs are an attractive target for cancer immunotherapy. Thereby, in this study we have analyzed if the developed Nut3a- and GM-CSF-loaded NPs could influence the polarization of TAMs towards a more M1-like state. For this purpose, D7 triple co-culture MCTS were incubated with bare NPs, co-loaded

(Nut3a+GM-CSF) NPs, free Nut3a, free GM-CSF and only cell culture media, as a control, for 48 h. Afterwards, MCTS were collected, dissociated into single cell suspension and the $CD14^+$ macrophage population were analyzed for the ratio of expression of CD163 (M2 marker) and of CD86 (M1 marker) (Figure 7 and Figure S4).

In the control group (cell culture media), the ratio of CD163 to CD86 was 5.1±3.4, indicating a higher number of M2-like macrophages, which is correlated with lower overall survival in CRC [93]. This was expected as TAMs tend to be polarized to M2 macrophages in the TME [94], suggesting that both cancer cells and fibroblasts induce naïve macrophage differentiation into an anti-inflammatory state. Free Nut3a, at a concentration of 10 μM, could significantly upregulate CD86 and downregulate CD163, resulting in the reduction of CD163 to CD86 ratio to 1.1±0.5. Nut3a was previously shown to downregulate M2 gene expression, suppressing the M2 phenotype through a p53 dependent pathway. Finally, at the tested conditions, bare NPs and co-loaded NPs also diminished the ratio between $CD163^+$ and $CD86^+$ cells (to 2.1±0.9 and 2.7±1.1, respectively), although in a less extent than free Nut3a. The ability of these NPs to induce M1 polarization can possibly be explained as cationic NPs, including cationic dextran, have been shown to induce M1-like polarization and upregulation of CD86 [95].

At the tested conditions GM-CSF, which was shown to induce macrophages differentiation to a M1 state [96, 97], when incubated with MCTS both in free state or loaded in the NPs, did not impact macrophage polarization. It is hypothesized that the amount of GM-CSF used could have been insufficient in comparison to the amounts used in other study [96] to produce any effect. Moreover, Notwithstanding, in that study, TAMs became more pro-inflammatory *ex vivo*, in absence of the pressure herein imposed by the MCTS tumor microenvironment, sustained by tumor cells and fibroblasts

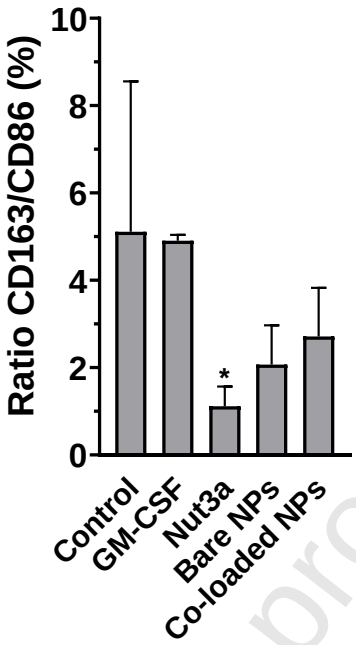

Figure 7. Macrophage polarization status. Ratio of CD163+ (M2 marker) to CD86+ (M1 marker) after incubating the triple culture MCTS with media (control), free GM-CSF, free Nut3a, bare NPs and co-loaded NPs for 48 h. Samples were analyzed with one-way ANOVA, followed by Dunnett's post-test. All results represent mean ± s.d. (n =2-4).

4. Conclusions

In this study, we have successfully developed a CRC–MCTS model constituted by three different cell populations, capable of recapitulating several aspects of the TME. The model was

constituted by human epithelial colon cancer cells, fibroblasts and primary monocytes, which could differentiate into macrophages. This CRC model mimicked different features of the tumor, such as ECM production, spatial organization, formation of a necrotic core, and ability to differentiate and polarize monocytes to M2-like macrophages. Furthermore, the method of production of this model is beneficial for high throughput screening, being adequate for drug screening and testing of nanoparticles and chemoimmunotherapy strategies for CRC treatment. The developed Sp-AcDEX NPs were biocompatible and successfully taken-up by the epithelial cells in both 2D monolayers and in the developed MCTS, despite in a significant lower extent in the later one. However, when loaded with Nut3a, these NPs showed an anti-proliferative effect both in 2D monolayers and in a higher extent in the developed CRC–MCTS model. Finally, when in contact with MCTS, Nut3a influenced the macrophage polarization to M1-like phenotype.

Acknowledgements

T. Bauleth-Ramos acknowledges financial support from Fundação para a Ciência e a Tecnologia (grant no. SFRH/BD/110859/2015). This work was financed by the project NORTE-01-0145-FEDER-000012 by Norte Portugal Regional Operational Programme (NORTE 2020), and COMPETE 2020 - Operacional Programme for Competitiveness and Internationalisation (POCI), under the PORTUGAL 2020 Partnership Agreement, through the FEDER - Fundo Europeu de Desenvolvimento Regional, and by Portuguese funds through FCT - Fundação para a Ciência e a Tecnologia/ Ministério da Ciência, Tecnologia e Ensino Superior in the framework of the project "Institute for Research and Innovation in Health Sciences" UID/BIM/04293/2019. M.-A.S. acknowledges financial support from the Academy of Finland (Decision No. 317316). Prof. H. A. Santos acknowledges financial support from the HiLIFE Research Funds, the Sigrid

Jusélius Foundation (Decision no. 4704580), and the European Research Council Prof-of-Concept Research Grant (Grant no. 4100164).

The authors acknowledge the support of the i3S Scientific Platforms: Advanced Light Microscopy (ALM) and Histology and Electron Microscopy, members of the national infrastructure PPBI - Portuguese Platform of Bioimaging (PPBI-POCI-01-0145-FEDER-022122). The authors also acknowledge the i3S Scientific Platform Biointerfaces and Nanotechnology (BN). and the Serviço de Imunohemoterapia of Centro Hospitalar Universitário de São João (CHUSJ), for kindly donating human Buffy Coats for primary monocytes isolation. The authors thank INEB histology technician Cláudia Machado for providing assistance with histology samples preparation.

References

[1] F. Bray, J. Ferlay, I. Soerjomataram, R.L. Siegel, L.A. Torre, A. Jemal, Global cancer statistics 2018: GLOBOCAN estimates of incidence and mortality worldwide for 36 cancers in 185 countries, CA Cancer J Clin, 68 (2018) 394-424.10.3322/caac.21492

[2] I. Jawed, J. Wilkerson, V. Prasad, A.G. Duffy, T. Fojo, Colorectal Cancer Survival Gains and Novel Treatment Regimens: A Systematic Review and Analysis, JAMA Oncology, 1 (2015) 787-795.10.1001/jamaoncol.2015.1790

[3] K.K. Ciombor, C. Wu, R.M. Goldberg, Recent Therapeutic Advances in the Treatment of Colorectal Cancer, Annu. Rev. Med., 66 (2015) 83-95.10.1146/annurev-med-051513-102539

[4] R.L. Siegel, K.D. Miller, S.A. Fedewa, D.J. Ahnen, R.G.S. Meester, A. Barzi, A. Jemal, Colorectal cancer statistics, 2017, CA Cancer J. Clin., 67 (2017) 177-193.10.3322/caac.21395

[5] M.C. Ocaña, B. Martínez-Poveda, A.R. Quesada, M.Á. Medina, Metabolism within the tumor microenvironment and its implication on cancer progression: An ongoing therapeutic target, Med. Res. Rev., 39 (2019) 70-113.10.1002/med.21511

[6] D. Hanahan, L.M. Coussens, Accessories to the crime: functions of cells recruited to the tumor microenvironment, Cancer Cell, 21 (2012) 309-322.10.1016/j.ccr.2012.02.022

[7] T. Chanmee, P. Ontong, K. Konno, N. Itano, Tumor-associated macrophages as major players in the tumor microenvironment, Cancers (Basel), 6 (2014) 1670-1690.10.3390/cancers6031670

[8] X. Zhong, B. Chen, Z. Yang, The Role of Tumor-Associated Macrophages in Colorectal Carcinoma Progression, Cell. Physiol. Biochem., 45 (2018) 356-365.10.1159/000486816

[9] X. Zhong, B. Chen, Z. Yang, The Role of Tumor-Associated Macrophages in Colorectal Carcinoma Progression, Cell. Physiol. Biochem., 45 (2018) 356-365.10.1159/000486816

[10] P.J. Murray, T.A. Wynn, Protective and pathogenic functions of macrophage subsets, Nat. Rev. Immunol., 11 (2011) 723-737.10.1038/nri3073

[11] L. Li, D.S. Ng, W.C. Mak, F.F. Almeida, S.A. Rahmat, V.K. Rao, S.C. Leow, F. Laudisi, M.T. Peh, A.M. Goh, J.S. Lim, G.D. Wright, A. Mortellaro, R. Taneja, F. Ginhoux, C.G. Lee, P.K. Moore, D.P. Lane, A unique role for p53 in the regulation of M2 macrophage polarization, Cell Death Differ., 22 (2015) 1081-1093.10.1038/cdd.2014.212

[12] M.S. Braun, M.T. Seymour, Balancing the efficacy and toxicity of chemotherapy in colorectal cancer, Ther Adv Med Oncol, 3 (2011) 43-52.10.1177/1758834010388342

[13] A.I. Matos, B. Carreira, C. Peres, L.I.F. Moura, J. Conniot, T. Fourniols, A. Scomparin, Á. Martínez-Barriocanal, D. Arango, J.P. Conde, V. Préat, R. Satchi-Fainaro, H.F. Florindo, Nanotechnology is an important strategy for combinational innovative chemo-immunotherapies

against colorectal cancer, J. Control. Release, 307 (2019) 108-138.https://doi.org/10.1016/j.jconrel.2019.06.017

[14] X.Y. Guo, P. Wang, Q.G. Du, S. Han, S.M. Zhu, Y.F. Lv, G.S. Liu, Z.M. Hao, Paclitaxel and gemcitabine combinational drug-loaded mucoadhesive delivery system in the treatment of colon cancers, Drug Res (Stuttg), 65 (2015) 199-204.10.1055/s-0034-1375665

[15] L. Bracci, G. Schiavoni, A. Sistigu, F. Belardelli, Immune-based mechanisms of cytotoxic chemotherapy: implications for the design of novel and rationale-based combined treatments against cancer, Cell Death Differ., 21 (2014) 15-25.10.1038/cdd.2013.67

[16] T. MIYASHITA, H. TAJIMA, I. MAKINO, M. OKAZAKI, T. YAMAGUCHI, Y. OHBATAKE, S. NAKANUMA, H. HAYASHI, H. TAKAMURA, I. NINOMIYA, S. FUSHIDA, K. KISHIMOTO, J.W. HARMON, T. OHTA, Neoadjuvant Chemotherapy with Gemcitabine Plus Nab-paclitaxel Reduces the Number of Cancer-associated Fibroblasts Through Depletion of Pancreatic Stroma, Anticancer Res., 38 (2018) 337-343

[17] C.G. Da Silva, M.G.M. Camps, T. Li, L. Zerrillo, C.W. Lowik, F. Ossendorp, L.J. Cruz, Effective chemoimmunotherapy by co-delivery of doxorubicin and immune adjuvants in biodegradable nanoparticles, Theranostics, 9 (2019) 6485-6500.10.7150/thno.34429

[18] M.S. Goldberg, Improving cancer immunotherapy through nanotechnology, Nature Reviews Cancer, 19 (2019) 587-602.10.1038/s41568-019-0186-9

[19] N. Niu, L. Wang, In vitro human cell line models to predict clinical response to anticancer drugs, Pharmacogenomics, 16 (2015) 273-285.10.2217/pgs.14.170

[20] A.S. Nunes, A.S. Barros, E.C. Costa, A.F. Moreira, I.J. Correia, 3D tumor spheroids as in vitro models to mimic in vivo human solid tumors resistance to therapeutic drugs, Biotechnol. Bioeng., 116 (2019) 206-226.10.1002/bit.26845

[21] P. Horvath, N. Aulner, M. Bickle, A.M. Davies, E.D. Nery, D. Ebner, M.C. Montoya, P. Ostling, V. Pietiainen, L.S. Price, S.L. Shorte, G. Turcatti, C. von Schantz, N.O. Carragher, Screening out irrelevant cell-based models of disease, Nat Rev Drug Discov, 15 (2016) 751-769.10.1038/nrd.2016.175

[22] J. Mestas, C.C.W. Hughes, Of Mice and Not Men: Differences between Mouse and Human Immunology, The Journal of Immunology, 172 (2004) 2731-2738.10.4049/jimmunol.172.5.2731

[23] G. Mehta, A.Y. Hsiao, M. Ingram, G.D. Luker, S. Takayama, Opportunities and challenges for use of tumor spheroids as models to test drug delivery and efficacy, J. Control. Release, 164 (2012) 192-204.https://doi.org/10.1016/j.jconrel.2012.04.045

[24] M. Majety, L.P. Pradel, M. Gies, C.H. Ries, Fibroblasts Influence Survival and Therapeutic Response in a 3D Co-Culture Model, PLoS One, 10 (2015) e0127948.10.1371/journal.pone.0127948

[25] J.W. Lee, D.H. Shin, J.L. Roh, Development of an in vitro cell-sheet cancer model for chemotherapeutic screening, Theranostics, 8 (2018) 3964-3973.10.7150/thno.26439

[26] M.E. Katt, A.L. Placone, A.D. Wong, Z.S. Xu, P.C. Searson, In Vitro Tumor Models: Advantages, Disadvantages, Variables, and Selecting the Right Platform, Frontiers in Bioengineering and Biotechnology, 4 (2016).10.3389/fbioe.2016.00012

[27] J.P. Ward, J.R. King, Mathematical modelling of avascular-tumour growth, IMA J Math Appl Med Biol, 14 (1997) 39-69

[28] H.M. Byrne, Dissecting cancer through mathematics: from the cell to the animal model, Nature Reviews Cancer, 10 (2010) 221-230.10.1038/nrc2808

[29] E.C. Costa, V.M. Gaspar, P. Coutinho, I.J. Correia, Optimization of liquid overlay technique to formulate heterogenic 3D co-cultures models, Biotechnology and Bioengineering, 111 (2014) 1672-1685.10.1002/bit.25210

[30] M. Millard, I. Yakavets, V. Zorin, A. Kulmukhamedova, S. Marchal, L. Bezdetnaya, Drug delivery to solid tumors: the predictive value of the multicellular tumor spheroid model for nanomedicine screening, International journal of nanomedicine, 12 (2017) 7993-8007.10.2147/IJN.S146927

[31] T. Bauleth-Ramos, M.-A. Shahbazi, D. Liu, F. Fontana, A. Correia, P. Figueiredo, H. Zhang, J.P. Martins, J.T. Hirvonen, P. Granja, B. Sarmento, H.A. Santos, Nutlin-3a and Cytokine Co-loaded Spermine-Modified Acetalated Dextran Nanoparticles for Cancer Chemo-Immunotherapy, Advanced Functional Materials 27 (2017) 1703303.10.1002/adfm.201703303

[32] K.E. Broaders, J.A. Cohen, T.T. Beaudette, E.M. Bachelder, J.M.J. Fréchet, Acetalated dextran is a chemically and biologically tunable material for particulate immunotherapy, Proceedings of the National Academy of Sciences, 106 (2009) 5497-5502.10.1073/pnas.0901592106

[33] E.M. Bachelder, T.T. Beaudette, K.E. Broaders, J. Dashe, J.M.J. Frechet, Acetal-derivatized dextran: An acid-responsive biodegradable material for therapeutic applications, J. Am. Chem. Soc., 130 (2008) 10494-+.10.1021/ja803947s

[34] J.L. Cohen, S. Schubert, P.R. Wich, L. Cui, J.A. Cohen, J.L. Mynar, J.M. Frechet, Acid-degradable cationic dextran particles for the delivery of siRNA therapeutics, Bioconjug. Chem., 22 (2011) 1056-1065.10.1021/bc100542r

[35] U. Bilati, E. Allemann, E. Doelker, Sonication parameters for the preparation of biodegradable nanocapsules of controlled size by the double emulsion method, Pharm. Dev. Technol., 8 (2003) 1-9.10.1081/PDT-120017517

[36] E. Bauman, T. Feijao, D.T.O. Carvalho, P.L. Granja, C.C. Barrias, Xeno-free pre-vascularized spheroids for therapeutic applications, Sci. Rep., 8 (2018) 230.10.1038/s41598-017-18431-6

[37] S.P.M. Crouch, R. Kozlowski, K.J. Slater, J. Fletcher, The use of ATP bioluminescence as a measure of cell proliferation and cytotoxicity, J. Immunol. Methods, 160 (1993) 81-88.https://doi.org/10.1016/0022-1759(93)90011-U

[38] H. Shoval, A. Karsch-Bluman, Y. Brill-Karniely, T. Stern, G. Zamir, A. Hubert, O. Benny, Tumor cells and their crosstalk with endothelial cells in 3D spheroids, Sci. Rep., 7 (2017) 10428.10.1038/s41598-017-10699-y

[39] C.R. Thoma, M. Zimmermann, I. Agarkova, J.M. Kelm, W. Krek, 3D cell culture systems modeling tumor growth determinants in cancer target discovery, Adv Drug Deliv Rev, 69-70 (2014) 29-41.10.1016/j.addr.2014.03.001

[40] B.W. Huang, J.Q. Gao, Application of 3D cultured multicellular spheroid tumor models in tumor-targeted drug delivery system research, J. Control. Release, 270 (2018) 246-259.10.1016/j.jconrel.2017.12.005

[41] O. Costăchel, L. Fadei, E. Badea, Tumor cell suspension culture on non adhesive substratum, Z. Krebsforsch., 72 (1969) 24-31.10.1007/bf00524788

[42] J.M. Yuhas, A.P. Li, A.O. Martinez, A.J. Ladman, A Simplified Method for Production and Growth of Multicellular Tumor Spheroids, Cancer Res., 37 (1977) 3639-3643

[43] E.C. Costa, D. de Melo-Diogo, A.F. Moreira, M.P. Carvalho, I.J. Correia, Spheroids Formation on Non-Adhesive Surfaces by Liquid Overlay Technique: Considerations and Practical Approaches, Biotechnol. J., 13 (2018) 1700417.10.1002/biot.201700417

[44] R.M. Sutherland, J.A. McCredie, W.R. Inch, Growth of Multicell Spheroids in Tissue Culture as a Model of Nodular Carcinomas2, JNCI: Journal of the National Cancer Institute, 46 (1971) 113-120.10.1093/jnci/46.1.113

[45] K.S.P. Devi, D. Mishra, B. Roy, S.K. Ghosh, T.K. Maiti, Assessing the immunomodulatory role of heteroglycan in a tumor spheroid and macrophage co-culture model system, Carbohydrate Polymers, 127 (2015) 1-10.https://doi.org/10.1016/j.carbpol.2015.03.035

[46] S.A. Elmore, D. Dixon, J.R. Hailey, T. Harada, R.A. Herbert, R.R. Maronpot, T. Nolte, J.E. Rehg, S. Rittinghausen, T.J. Rosol, H. Satoh, J.D. Vidal, C.L. Willard-Mack, D.M. Creasy, Recommendations from the INHAND Apoptosis/Necrosis Working Group, Toxicol. Pathol., 44 (2016) 173-188.10.1177/0192623315623859

[47] P. Vandenabeele, L. Galluzzi, T. Vanden Berghe, G. Kroemer, Molecular mechanisms of necroptosis: an ordered cellular explosion, Nature Reviews Molecular Cell Biology, 11 (2010) 700-714.10.1038/nrm2970

[48] H. Lu, M.H. Stenzel, Multicellular Tumor Spheroids (MCTS) as a 3D In Vitro Evaluation Tool of Nanoparticles, Small, 14 (2018) 1702858.10.1002/smll.201702858

[49] C. Gebhard, C. Gabriel, I. Walter, Morphological and Immunohistochemical Characterization of Canine Osteosarcoma Spheroid Cell Cultures, Anat. Histol. Embryol., 45 (2016) 219-230.10.1111/ahe.12190

[50] L.A. Kunz-Schughart, J.P. Freyer, F. Hofstaedter, R. Ebner, The Use of 3-D Cultures for High-Throughput Screening: The Multicellular Spheroid Model, J. Biomol. Screen., 9 (2004) 273-285.10.1177/1087057104265040

[51] R.-Z. Lin, H.-Y. Chang, Recent advances in three-dimensional multicellular spheroid culture for biomedical research, Biotechnol. J., 3 (2008) 1172-1184.10.1002/biot.200700228

[52] R. Kalluri, The biology and function of fibroblasts in cancer, Nature Reviews Cancer, 16 (2016) 582.10.1038/nrc.2016.73

[53] M.A. Kinney, T.A. Hookway, Y. Wang, T.C. McDevitt, Engineering three-dimensional stem cell morphogenesis for the development of tissue models and scalable regenerative therapeutics, Ann. Biomed. Eng., 42 (2014) 352-367.10.1007/s10439-013-0953-9

[54] R. Kalluri, M. Zeisberg, Fibroblasts in cancer, Nat. Rev. Cancer, 6 (2006) 392-401.10.1038/nrc1877

[55] D. Ohlund, E. Elyada, D. Tuveson, Fibroblast heterogeneity in the cancer wound, J. Exp. Med., 211 (2014) 1503-1523.10.1084/jem.20140692

[56] M. Romero-Lopez, A.L. Trinh, A. Sobrino, M.M. Hatch, M.T. Keating, C. Fimbres, D.E. Lewis, P.D. Gershon, E.L. Botvinick, M. Digman, J.S. Lowengrub, C.C. Hughes, Recapitulating the human tumor microenvironment: Colon tumor-derived extracellular matrix promotes angiogenesis and tumor cell growth, Biomaterials, 116 (2017) 118-129.10.1016/j.biomaterials.2016.11.034

[57] R. Ostuni, F. Kratochvill, P.J. Murray, G. Natoli, Macrophages and cancer: from mechanisms to therapeutic implications, Trends Immunol., 36 (2015) 229-239.10.1016/j.it.2015.02.004

[58] R. Zhang, F. Qi, F. Zhao, G. Li, S. Shao, X. Zhang, L. Yuan, Y. Feng, Cancer-associated fibroblasts enhance tumor-associated macrophages enrichment and suppress NK cells function in colorectal cancer, Cell Death Dis., 10 (2019) 273.10.1038/s41419-019-1435-2

[59] V.L. Silva, W.T. Al-Jamal, Exploiting the cancer niche: Tumor-associated macrophages and hypoxia as promising synergistic targets for nano-based therapy, J. Control. Release, 253 (2017) 82-96.https://doi.org/10.1016/j.jconrel.2017.03.013

[60] B.Z. Qian, J.W. Pollard, Macrophage diversity enhances tumor progression and metastasis, Cell, 141 (2010) 39-51.10.1016/j.cell.2010.03.014

[61] L. Bingle, N.J. Brown, C.E. Lewis, The role of tumour-associated macrophages in tumour progression: implications for new anticancer therapies. The Journal of Pathology, 196 (2002) 254-265.10.1002/path.1027

[62] K.S. Baghel, B.N. Tewari, R. Shrivastava, S.A. Malik, M.U.D. Lone, N.K. Jain, C. Tripathi, R.K. Kanchan, S. Dixit, K. Singh, K. Mitra, M.P.S. Negi, M. Srivastava, S. Misra, M.L.B. Bhatt, S. Bhadauria, Macrophages promote matrix protrusive and invasive function of breast cancer cells via MIP-1β dependent upregulation of MYO3A gene in breast cancer cells, Oncoimmunology, 5 (2016) e1196299.10.1080/2162402X.2016.1196299

[63] M.L. Pinto, E. Rios, C. Durães, R. Ribeiro, J.C. Machado, A. Mantovani, M.A. Barbosa, F. Carneiro, M.J. Oliveira, The Two Faces of Tumor-Associated Macrophages and Their Clinical Significance in Colorectal Cancer, Frontiers in Immunology, 10 (2019).10.3389/fimmu.2019.01875

[64] C. Wei, C. Yang, S. Wang, D. Shi, C. Zhang, X. Lin, Q. Liu, R. Dou, B. Xiong, Crosstalk between cancer cells and tumor associated macrophages is required for mesenchymal circulating

tumor cell-mediated colorectal cancer metastasis, Molecular Cancer, 18 (2019) 64.10.1186/s12943-019-0976-4

[65] T. Bauleth-Ramos, T.-Y. Shih, M.-A. Shahbazi, A.J. Najibi, A.S. Mao, D. Liu, P. Granja, H.A. Santos, B. Sarmento, D.J. Mooney, Acetalated Dextran Nanoparticles Loaded into an Injectable Alginate Cryogel for Combined Chemotherapy and Cancer Vaccination, Advanced Functional Materials, 29 (2019) 1903686.10.1002/adfm.201903686

[66] F. Fontana, M.-A. Shahbazi, D. Liu, H. Zhang, E. Mäkilä, J. Salonen, J.T. Hirvonen, H.A. Santos, Multistaged Nanovaccines Based on Porous Silicon@Acetalated Dextran@Cancer Cell Membrane for Cancer Immunotherapy, Advanced Materials, 29 (2017) 1603239.10.1002/adma.201603239

[67] Y. Li, J. Wang, M.G. Wientjes, J.L.S. Au, Delivery of nanomedicines to extracellular and intracellular compartments of a solid tumor, Advanced Drug Delivery Reviews, 64 (2012) 29-39.https://doi.org/10.1016/j.addr.2011.04.006

[68] A. Ozcelikkale, S. Ghosh, B. Han, Multifaceted Transport Characteristics of Nanomedicine: Needs for Characterization in Dynamic Environment, Mol. Pharm., 10 (2013) 2111-2126.10.1021/mp3005947

[69] W. Rao, H. Wang, J. Han, S. Zhao, J. Dumbleton, P. Agarwal, W. Zhang, G. Zhao, J. Yu, D.L. Zynger, X. Lu, X. He, Chitosan-Decorated Doxorubicin-Encapsulated Nanoparticle Targets and Eliminates Tumor Reinitiating Cancer Stem-like Cells, ACS Nano, 9 (2015) 5725-5740.10.1021/nn506928p

[70] M. Björnmalm, K.J. Thurecht, M. Michael, A.M. Scott, F. Caruso, Bridging Bio–Nano Science and Cancer Nanomedicine, ACS Nano, 11 (2017) 9594-9613.10.1021/acsnano.7b04855

[71] X. Guo, Z. Wu, W. Li, Z. Wang, Q. Li, F. Kong, H. Zhang, X. Zhu, Y.P. Du, Y. Jin, Y. Du, J. You, Appropriate Size of Magnetic Nanoparticles for Various Bioapplications in Cancer Diagnostics and Therapy, ACS Applied Materials & Interfaces, 8 (2016) 3092-3106.10.1021/acsami.5b10352

[72] A. Tchoryk, V. Taresco, R.H. Argent, M. Ashford, P.R. Gellert, S. Stolnik, A. Grabowska, M.C. Garnett, Penetration and Uptake of Nanoparticles in 3D Tumor Spheroids, Bioconjug. Chem., 30 (2019) 1371-1384.10.1021/acs.bioconjchem.9b00136

[73] M.A. Solomon, J. Lemera, G.G.M. D'Souza, Development of an in vitro tumor spheroid culture model amenable to high-throughput testing of potential anticancer nanotherapeutics, Journal of Liposome Research, 26 (2016) 246-260.10.3109/08982104.2015.1105820

[74] H.H. Gustafson, D. Holt-Casper, D.W. Grainger, H. Ghandehari, Nanoparticle Uptake: The Phagocyte Problem, Nano today, 10 (2015) 487-510.10.1016/j.nantod.2015.06.006

[75] S. Lanone, F. Rogerieux, J. Geys, A. Dupont, E. Maillot-Marechal, J. Boczkowski, G. Lacroix, P. Hoet, Comparative toxicity of 24 manufactured nanoparticles in human alveolar epithelial and macrophage cell lines, Part. Fibre Toxicol., 6 (2009) 14.10.1186/1743-8977-6-14

[76] L. Ma, T.W. Liu, M.A. Wallig, I.T. Dobrucki, L.W. Dobrucki, E.R. Nelson, K.S. Swanson, A.M. Smith, Efficient Targeting of Adipose Tissue Macrophages in Obesity with Polysaccharide Nanocarriers, ACS Nano, 10 (2016) 6952-6962.10.1021/acsnano.6b02878

[77] S. Pustylnikov, D. Sagar, P. Jain, Z.K. Khan, Targeting the C-type lectins-mediated host-pathogen interactions with dextran, J. Pharm. Pharm. Sci., 17 (2014) 371-392

[78] G. Hu, M. Guo, J. Xu, F. Wu, J. Fan, Q. Huang, G. Yang, Z. Lv, X. Wang, Y. Jin, Nanoparticles Targeting Macrophages as Potential Clinical Therapeutic Agents Against Cancer and Inflammation, Front. Immunol., 10 (2019).10.3389/fimmu.2019.01998

[79] X.L. Li, J. Zhou, Z.R. Chen, W.J. Chng, P53 mutations in colorectal cancer - molecular pathogenesis and pharmacological reactivation, World J. Gastroenterol., 21 (2015) 84-93.10.3748/wjg.v21.i1.84

[80] P. Secchiero, R. Bosco, C. Celeghini, G. Zauli, Recent Advances in the Therapeutic Perspectives of Nutlin-3, Curr. Pharm. Des., 17 (2011) 569-577.Doi 10.2174/138161211795222586

[81] A.J. Levine, M. Oren, The first 30 years of p53: growing ever more complex, Nat. Rev. Cancer, 9 (2009) 749-758.10.1038/nrc2723

[82] T. Takayama, K. Miyanishi, T. Hayashi, Y. Sato, Y. Niitsu, Colorectal cancer: genetics of development and metastasis, J. Gastroenterol., 41 (2006) 185-192.10.1007/s00535-006-1801-6

[83] L.N. Micel, J.J. Tentler, P.G. Smith, G.S. Eckhardt, Role of ubiquitin ligases and the proteasome in oncogenesis: novel targets for anticancer therapies, J. Clin. Oncol., 31 (2013) 1231-1238.10.1200/JCO.2012.44.0958

[84] M.J. Rigatti, R. Verma, G.S. Belinsky, D.W. Rosenberg, C. Giardina, Pharmacological inhibition of Mdm2 triggers growth arrest and promotes DNA breakage in mouse colon tumors and human colon cancer cells, Mol. Carcinog., 51 (2012) 363-378.10.1002/mc.20795

[85] A. Efeyan, A. Ortega-Molina, S. Velasco-Miguel, D. Herranz, L.T. Vassilev, M. Serrano, Induction of p53-Dependent Senescence by the MDM2 Antagonist Nutlin-3a in Mouse Cells of Fibroblast Origin, Cancer Res., 67 (2007) 7350-7357.10.1158/0008-5472.Can-07-0200

[86] K. Kumamoto, E.A. Spillare, K. Fujita, I. Horikawa, T. Yamashita, E. Appella, M. Nagashima, S. Takenoshita, J. Yokota, C.C. Harris, Nutlin-3a activates p53 to both down-regulate inhibitor of growth 2 and up-regulate mir-34a, mir-34b, and mir-34c expression, and induce senescence, Cancer Res., 68 (2008) 3193-3203.10.1158/0008-5472.CAN-07-2780

[87] D.M. Lee, I.Y. Kim, M.J. Seo, M.R. Kwon, K.S. Choi, Nutlin-3 enhances the bortezomib sensitivity of p53-defective cancer cells by inducing paraptosis, Exp. Mol. Med., 49 (2017) e365-e365.10.1038/emm.2017.112

[88] T. Hori, T. Kondo, M. Kanamori, Y. Tabuchi, R. Ogawa, Q.-L. Zhao, K. Ahmed, T. Yasuda, S. Seki, K. Suzuki, T. Kimura, Nutlin-3 enhances tumor necrosis factor-related apoptosis-inducing ligand (TRAIL)-induced apoptosis through up-regulation of death receptor 5 (DR5) in human sarcoma HOS cells and human colon cancer HCT116 cells, Cancer Lett., 287 (2010) 98-108.https://doi.org/10.1016/j.canlet.2009.06.002

[89] D.F. Liu, H.B. Zhang, E. Makila, J. Fan, B. Herranz-Blanco, C.F. Wang, R. Rosa, A.J. Ribeiro, J. Salonen, J. Hirvonen, H.A. Santos, Microfluidic assisted one-step fabrication of porous silicon@acetalated dextran nanocomposites for precisely controlled combination chemotherapy, Biomaterials, 39 (2015) 249-259.10.1016/j.biomaterials.2014.10.079

[90] H. Janouskova, A.-M. Ray, F. Noulet, I. Lelong-Rebel, L. Choulier, F. Schaffner, M. Lehmann, S. Martin, J. Teisinger, M. Dontenwill, Activation of p53 pathway by Nutlin-3a inhibits the expression of the therapeutic target α5 integrin in colon cancer cells, Cancer Lett., 336 (2013) 307-318.https://doi.org/10.1016/j.canlet.2013.03.018

[91] J. Gong, D. Wang, L. Sun, E. Zborowska, J. Willson, M. Brattain, Role of alpha 5 beta 1 integrin in determining malignant properties of colon carcinoma cells, Cell Growth Differ., 8 (1997) 83-90

[92] T. Koike, N. Kimura, K. Miyazaki, T. Yabuta, K. Kumamoto, S. Takenoshita, J. Chen, M. Kobayashi, M. Hosokawa, A. Taniguchi, T. Kojima, N. Ishida, M. Kawakita, H. Yamamoto, H. Takematsu, A. Suzuki, Y. Kozutsumi, R. Kanangi, Hypoxia induces adhesion molecules on

cancer cells: A missing link between Warburg effect and induction of selectin-ligand carbohydrates, Proc. Natl. Acad. Sci. U. S. A., 101 (2004) 8132-8137.10.1073/pnas.0402088101

[93] M.L. Pinto, E. Rios, C. Durães, R. Ribeiro, J.C. Machado, A. Mantovani, M.A. Barbosa, F. Carneiro, M.J. Oliveira, The two faces of tumor-associated macrophages and their clinical significance in colorectal cancer, Front. Immunol., 10 (2019).10.3389/fimmu.2019.01875

[94] M.A.F. Yahaya, M.A.M. Lila, S. Ismail, M. Zainol, N.A.R.N.M. Afizan, Tumour-Associated Macrophages (TAMs) in Colon Cancer and How to Reeducate Them, Journal of immunology research, 2019 (2019) 2368249-2368249.10.1155/2019/2368249

[95] Z. Huang, Y. Yang, Y. Jiang, J. Shao, X. Sun, J. Chen, L. Dong, J. Zhang, Anti-tumor immune responses of tumor-associated macrophages via toll-like receptor 4 triggered by cationic polymers, Biomaterials, 34 (2013) 746-755.10.1016/j.biomaterials.2012.09.062

[96] T. Krausgruber, K. Blazek, T. Smallie, S. Alzabin, H. Lockstone, N. Sahgal, T. Hussell, M. Feldmann, I.A. Udalova, IRF5 promotes inflammatory macrophage polarization and TH1-TH17 responses, Nature Immunology, 12 (2011) 231-238.10.1038/ni.1990

[97] T. Lawrence, G. Natoli, Transcriptional regulation of macrophage polarization: enabling diversity with identity, Nature Reviews Immunology, 11 (2011) 750-761.10.1038/nri3088

Author's statement

Tomás Bauleth-Ramos: Conceptualization, Methodology, Writing

Tália Feijão: Conceptualization, Methodology

André Gonçalves: Conceptualization, Methodology, Writing

Mohammad-Ali Shahbazi: Conceptualization, Methodology, Writing

Zehua Liu: Methodology

Cristina Barrias: Writing, Reviewing and Editing

Maria José Oliveira: Writing, Reviewing and Editing

Pedro Granja.: Conceptualization

Hélder Santos: Conceptualization, Writing, Editing

Bruno Sarmento: Conceptualization, Writing, Editing